HHS Public Access

Author manuscript

J Neural Eng. Author manuscript; available in PMC 2016 May 03.

Published in final edited form as:

J Neural Eng. 2016 April ; 13(2): 026003. doi:10.1088/1741-2560/13/2/026003.

Scanning electron microscopy of chronically implanted intracortical microelectrode arrays in non-human primates

James C Barrese[1,2], **Juan Aceros**[3,4], and **John P Donoghue**[2]

[1] Department of Neurological Surgery, New Jersey Medical School, Rutgers University, Newark, New Jersey, USA

[2] Department of Neuroscience and Brown Institute for Brain Science, Brown University, Providence, Rhode Island, USA

[3] School of Engineering, Brown University, Providence, Rhode Island, USA

[4] School of Engineering, University of North Florida, Jacksonville, Florida, USA

Abstract

Objective—Signal attenuation is a major problem facing intracortical sensors for chronic neuroprosthetic applications. Many studies suggest that failure is due to gliosis around the electrode tips, however, mechanical and material causes of failure are often overlooked. The purpose of this study was to investigate the factors contributing to progressive signal decline by using scanning electron microscopy (SEM) to visualize structural changes in chronically implanted arrays and histology to examine the tissue response at corresponding implant sites.

Approach—We examined eight chronically implanted intracortical microelectrode arrays (MEAs) explanted from non-human primates at times ranging from 37 to 1051 days post-implant. We used SEM, *in vivo* neural recordings, and histology (GFAP, Iba-1, NeuN). Three MEAs that were never implanted were also imaged as controls.

Main results—SEM revealed progressive corrosion of the platinum electrode tips and changes to the underlying silicon. The parylene insulation was prone to cracking and delamination, and in some instances the silicone elastomer also delaminated from the edges of the MEA. Substantial tissue encapsulation was observed and was often seen growing into defects in the platinum and parylene. These material defects became more common as the time *in vivo* increased. Histology at 37 and 1051 days post-implant showed gliosis, disruption of normal cortical architecture with minimal neuronal loss, and high Iba-1 reactivity, especially within the arachnoid and dura. Electrode tracts were either absent or barely visible in the cortex at 1051 days, but were seen in the fibrotic encapsulation material suggesting that the MEAs were lifted out of the brain. Neural recordings showed a progressive drop in impedance, signal amplitude, and viable channels over time.

Significance—These results provide evidence that signal loss in MEAs is truly multifactorial. Gliosis occurs in the first few months after implantation but does not prevent useful recordings for several years. Progressive meningeal fibrosis encapsulates and lifts MEAs out of the cortex while

jamesbarresemd@gmail.com

ongoing foreign body reactions lead to progressive degradation of the materials. Long-term impedance drops are due to the corrosion of platinum, cracking and delamination of parylene, and delamination of silicone elastomer. Oxygen radicals released by cells of the immune system likely mediate the degradation of these materials. Future MEA designs must address these problems through more durable insulation materials, more inert electrode alloys, and pharmacologic suppression of fibroblasts and leukocytes.

Keywords

neuroprosthetics; brain–computer interfaces; scanning electron microscopy; microelectrode failures; chronic neural recordings; gliosis

1. Introduction

Neuroprosthetic devices, also known as brain–computer interfaces (BCI), have enormous potential for the restoration of neurological function. Disabled individuals will one day regain their mobility and independence through the use of such devices. BCI's utilize sensors that record neuronal activity with high temporal and spatial resolution across large populations of neurons. In order to capture sufficient neural data, intracortical microelectrode arrays (MEA's) capable of recording single-unit activity are often the sensor of choice [1]. These neural signals are transmitted to a computer that interprets the data, and converts it into a functional output [2, 3]. The output may be used to control a robotic arm, computer cursor, or functional electrical stimulation system [4–10].

Despite considerable technological advancements in the field of BCI, an intracortical MEA that will function reliably for at least a decade of clinical use has yet to be designed. Numerous animals studies have demonstrated that signals recorded from these systems fade over time, eventually leading to sensor failure and loss of neural recordings [11–19]. Consequently, researchers have started investigating the factors that contribute to long-term recording failure [13, 16, 20–24].

While tissue response to the electrodes has been well studied, the particular mechanisms that lead to recording failure are still largely unidentified and poorly understood [25]. Proposed mechanisms include foreign body reactions causing device migration, gliosis, neuronal migration, and neuronal inflammation and death [26–32]. Fibrotic tissue encapsulation as well might be a major factor [12, 20, 33–36]. Previous research has indicated that fibroblasts have an increased ability to attach and spread along flat, ionized parylene-C surfaces in the presence of serum proteins [34]. The growth of infiltrating fibroblasts from the meninges (arachnoid or dura) re-establish the intraparenchymal and extraparenchymal boundary and neurothelial cells from the subdural space generate a glia-limitans like membrane [37, 38]. Progressive meningeal growth that gradually lifts the array out of the cortex likely explains some of the observed signal loss. The types of material failures and their role in signal attenuation have not been studied in detail and are often overlooked, as signal attenuation has primarily been attributed to biological causes. Material failures may involve the dielectric materials used for encapsulation, i.e. parylene or silicone cracking or delamination, or the decomposition of the metallic electrodes, i.e. platinum or iridium oxide

degradation. In a recently published MEA failure mode analysis, our group proposed that materials degradation secondary to an aggressive foreign body reaction is a primary underlying cause of the time-related decline in signal quality and viable channel (VC) count [20]. Growth of fibrous meningeal scar tissue that encapsulates the array and pulls it out of the brain was also identified as a major barrier to successful long-term functioning of MEAs.

In this report we present scanning electron micrographs of a series of chronically implanted intracortical MEAs following their explantation from non-human primates in order to identify potential failure modes. We expected to find evidence of fibrous meningeal encapsulation, but also wanted to determine the extent of the materials degradation that was suggested in our earlier work. With the ability to examine intricate structural details at the nanometer scale, scanning electron microscopy (SEM) imaging techniques have enabled us to directly observe the interactions between cells and biomaterials making SEM an ideal tool for the study of neuroprosthetic failure modes. We found further evidence supporting materials degradation as a significant impediment for long-term MEA success but also found evidence suggesting that this decay process is tied to a biological attack on the MEA, distinct from the process of gliosis. Specifically, we found that meningeal scar tissue fully encapsulates the MEA, lifting it out of the brain. Fibrous tissue was also found growing into cracks in both the parylene and platinum, further accelerating the breakdown of electrode materials. The findings of this report will help guide the development of more reliable neuroprosthetic sensors.

2. Materials and methods

Eight silicon MEAs were implanted in 5 monkeys (*Macaca mulatta*: 4 male, 1 female) as part of neuroscience graduate thesis work studying the organization of the motor cortex. The time *in vivo* for these experimental arrays ranged from 37 to 1051 days post-implant. The recording data used and analyzed in this retrospective study had research goals that did not include failure mode analysis and therefore recording intervals are not standardized between arrays and histology is not available for all specimens. Following explantation, the arrays were placed in a fixative for preservation and then imaged using a SEM. Three control arrays (never implanted, no recordings) were imaged as well.

2.1. Microelectrode arrays

MEAs form the physical interface between neurons and the electronic sensors employed for processing neural signals. The microelectrodes in these arrays consist of tissue penetrating shank microelectrodes through which the extracellular electrical neural activity can be detected and conveyed to the electronic circuitry for analysis. Although there are a variety of designs in use today, for this study we focused on Blackrock Microsystem's (BRMS) high-density, multi-channel MEAs (see figure 1). These arrays have microelectrode shanks typically implanted between 1 mm and 1.5 mm deep into the cortex of the brain. All arrays used in this study had 1 mm electrode shanks and were manufactured using a monolithic silicon (Si) micromachining process by BRMS (formerly known as Cyberkinetics). An array is composed of 100 microelectrodes, arranged in a 10 × 10 grid and isolated from each other using frit glass. Each individual shank microelectrode consists of boron-doped silicon that is

tapered via wet etching techniques to a point with 3–5 μm radius of curvature. The tip of the shank is metalized using a sputtered platinum (Pt) thin film. The base of each electrode shank is 80 μm in diameter, with each electrode spaced from each other at 400 μm intervals. The entire shank is coated with parylene-C, with the exception of the last ~30 μm at the tip, where the parylene is etched away using a plasma process. This allows for the metalized end of the tip to be exposed to the extracellular activity in the brain. The impedance of these arrays, as specified by the manufacturer, ranges from 200 kOhm to 800 kOhm at 1 kHz. Finally, the recorded signal from each electrode is linked to a percutaneous connector using gold wire bonds on the back of the array. Silicone elastomer is used to encapsulate the wire bond sites on the back of the array and overlaps the parylene encapsulation material on the edges of the array. Note that the three control arrays used in this study did not have silicone placed prior to imaging.

2.2. Surgical technique

2.2.1. Implantation—Eight arrays were implanted into 5 Rhesus Macaques (*Macaca mulatta*). There were 4 males and 1 female. All arrays reported in this study were implanted in compliance with Brown University's Institutional Animal Care and Use Committee (IACUC) policies on animal procedures. A general effort was made to mimic human neurosurgical protocols and procedures and to reduce the inclusion of foreign materials (e.g. epidural GoreTex, silastic, etc). For each procedure a mid-line skin incision was made and a small (less than 5 cm^2) craniotomy performed with a high-speed drill (Stryker, Kalamazoo, MI, USA). The craniotomy was kept as small as possible in order to minimize the risk of infection and CSF leak. The dura was then cut and reflected. All implants in this series were inserted using a custom pneumatic piston (insertion speed: 8–10 m s^{-1}), developed by the Normann lab at the University of Utah [39], and now manufactured by BRMS. A micromanipulator arm held the pneumatic inserter orthogonal to the array and excursion matched the array length at 1 mm.

A primary dural closure was performed using 4-0 Nurolon sutures (Ethicon, Inc., Somerville, NJ, USA), and a periosteal or fascial graft was used to close any remaining dural defects. Teflon, GoreTex, and silastic were not used for dural closure in any of the implants in this study, as foreign bodies are thought to lead to a higher rate of infections [20]. The bone flap was replaced and secured with a low profile titanium plating system (MatrixNeuro, Synthes, Inc., West Chester, PA, USA). In one case (LA-LMI4), titanium mesh was used to cover the craniotomy rather than replacing the bone flap, and dental acrylic was applied to secure the connector. Dental acrylic is generally avoided unless necessary to replace or repair an existing acrylic cap.

2.2.2. Explantation—Seven MEAs were surgically removed from healthy monkeys and placed in a NaCacodylate fixative for tissue preservation. Five of the seven arrays removed from living animals (SCT, RUS, GAR) were explanted in order for the monkey to be used in additional experiments. Two of the seven arrays were removed from a healthy monkey (LA) that was subsequently euthanized in order to obtain histology. Only one of the eight experimental arrays (LN-LSMA) was removed from the brain of a euthanized monkey after perfusion with NaCacodylate tissue fixative, then immediately placed into a separate

container with the same fixative. Microsurgical technique was used for all explantation procedures with care taken to avoid damage to the array or surrounding brain. For each procedure, the prior incision was opened and any existing cranial fixation hardware was removed. A high-speed drill (Stryker, Kalamazoo, MI, USA) was then used for the craniotomy. Bone immediately surrounding the connector wire was carefully removed with a Kerrison rongeur. In one case (LA-LMI4), the drill was used to remove dental acrylic, exposing the titanium mesh, which was then removed. Once the dura was exposed, it was cut and reflected along the length of the connector wire. The MEA was then identified within its fibrous capsule. Varying degrees of tissue encapsulation were encountered. The capsule was then sharply incised in a cruciate fashion and the leaflets were reflected. The MEA was gently lifted out of its tissue bed with forceps. Care was taken to remove the MEA without twisting or bending in order to prevent damage to the electrode tips or the surrounding tissue. Once the MEA was explanted, the leaflets were folded back into their original position and the dura was closed with 4-0 Nurolon sutures (Ethicon, Inc., Somerville, NJ, USA). The bone flap was replaced and secured with a low profile titanium plating system (MatrixNeuro, Synthes, Inc., West Chester, PA, USA). Next, the galea was closed with interrupted 3-0 Vicryl sutures (Ethicon, Inc., Somerville, NJ, USA) and the skin was closed with a running, subcuticular 4-0 Vicryl. See figure 2 for intra-operative photos of each array at the time of explantation.

2.3. Neural recordings

2.3.1. Neural data—Digital data was variably collected from 7 of the 8 experimental arrays. All of these arrays had 96 wire-bonded electrodes. The duration and frequency of recording between arrays was inconsistent as the goal of recording at the time was thesis work and not a failure mode analysis. The following methods (previously reported by our group) were applied for all implants with available digital recording data [20].

2.3.2. Signal-to-noise and amplitude calculations—For every channel on each recording day, all spike waveforms were aggregated to compute signal-to-noise ratios (SNR) and peak-to-peak (PTP) amplitude for that particular channel. Signals were first filtered with a single-pole analogue anti-aliasing filter with a 7.5 kHz cut-off frequency. The signal was then filtered using a fourth order Butterworth digital high-pass filter to extract spiking waveforms. This signal was sampled at 30 kHz. A neural spike was determined by this signal crossing a threshold typically set at −4.5 dB of the distribution of signal values, but this was not always the case (sometimes set manually). A spike waveform spans 1.6 ms or 48 samples. Ten of these samples were before the threshold crossing and 38 samples were after the threshold crossing. Any channel that had >150 threshold crossings over a recording session was considered active and was further analyzed.

SNR was calculated in two parts. The noise amplitude for a channel was determined by finding the maximum and minimum values of each of the first five samples of the 48-sample window for all threshold crossings (typically tens of thousands). Recall that the first five samples precede the threshold crossing and should be uncontaminated by the actual spike waveform, although occasional pretrigger inflections in the waveform may be included and could increase noise estimate. The noise amplitude is the max–min difference of the mean

over five points for all threshold crossings. We calculated the signal amplitude (PTP) by taking the median (across threshold crossings) of all samples and then finding the difference between the maximum and minimum of the median waveforms. The median was chosen in order to prevent large amplitude noise signals from artificially inflating the PTP. The ratio of the signal amplitude to the noise amplitude was the SNR.

2.3.3. Viable channels—The number of VCs per array for each recording session was then calculated. VCs were defined as individual electrodes (or 'channels') within an array that were capable of recording action potentials. A channel was considered viable if it had a PTP amplitude ≥40 μV, noise amplitude <150 μV, and SNR >1.

2.3.4. Impedance measurements—All impedance values reported in this analysis were measured using a commercial impedance meter designed for microelectrodes that is integrated into the BRMS Cerebus recording system (Blackrock Microsystems Inc., Salt Lake City, Utah, USA). The device applies a 1 kHz stimulus ±50 pA max, using the built-in capabilities of the NeuroPort hardware and Cerebus Central software.

2.4. Scanning electron microscopy

2.4.1. Experimental array fixation—Following explantation from the brain, all arrays were placed immediately into NaCacodylate fixative for at least 24 h and then progressively transitioned to 25%, 50%, 75%, and finally 100% ethanol. They were then dried in a critical point dryer using liquid CO_2. This process was performed to preserve and stabilize any biological samples on the arrays. All arrays except RUS-LPMv2 and RUS-LPFv2 were then sputter-coated with 30 nm of Au/Pd alloy before imaging to eliminate the accumulation of charge from electron ion bombardment on non-conductive samples during imaging.

2.4.2. Control array fixation—Three arrays, donated by BRMS for the purpose of this study, were used as controls for imaging. The arrays were manufactured in the same manner as the implanted arrays with the exception that the control arrays were not coated in silicone elastomer (PDMS). The silicone encapsulation only coats the back and sides of each array and therefore would not significantly affect the imaging results for the electrodes. In order to control for possible artifacts caused by the preservation process, each control array was processed in a slightly different manner. The first control array was not placed in any fixative solution. The second array was placed in NaCl for one week, and the third array was placed in NaCacodylate fixative for one week. The second and third arrays were then transferred to 25%, 50%, 75% and finally 100% ethanol at the end of 1 week to mimic the tissue preservation protocol used for the experimental arrays. All three arrays were then transferred to the critical point CO_2 dryer and processed in the same fashion as the implanted arrays. Once dried, the control arrays were sputter-coated with a 30 nm thin film of Au/Pd.

2.4.3. Imaging—All SEM images were taken using a LEO 1530 field emissions SEM. A standard 30 μm aperture was used with accelerating voltages varied from 1 kV up to 10 kV with most images taken at 5 kV. Working distance varied from 2 mm to 8 mm with most images taken at 5 mm. Arrays were imaged using an annular in-lens secondary electron detector.

2.5. Histology

Two of the monkeys used in this experiment (LN, LA) were euthanized in order to obtain histology. The first monkey (LN) was perfused at 37 days post-implant and the array was removed post-mortem. The other monkey (LA) had 2 arrays that were surgically removed a few hours prior to perfusion. One array (LA-LMI4) had been in place for 639 days and the other (LA-LPE3) for 1051 days. Both animals were euthanized according to IACUC protocol with sodium pento-barbital and perfused with NaCacodylate fixative. The brains were then removed, placed into containers of NaCacodylate fixative, and shipped to a commercial lab for slicing and staining (Neuroscience Associates, Knoxville, TN, USA). Both brains were freeze-sectioned at 40 μm in the coronal plane then stained with NeuN to show neurons, Iba1 to show activated microglia and macrophages, and GFAP to show astrocyte activity. Details of the staining process can be obtained from Neuroscience Associates upon request (www.neuroscienceassociates.com).

2.6. Failure mode classification

In a previous publication, we proposed a classification system for failure, which is defined as the absence of extractable action potentials for all electrodes (channels) on an array. Failures are characterized as acute or chronic, to distinguish catastrophic from progressive events, where acute failure is a rapid loss of signals within a time period of seven days and chronic failure is a slow, progressive loss of neural signals over a period of time longer than one week, typically years. Failures are also placed into four different categories: biological, material, mechanical, and unknown. Biological failures were defined as those related to the foreign body response of the tissue to the sensor or clinical issues arising from the implant such as infection or hemorrhage. Material failures were related to design flaws or material degradation. Mechanical failures were due to physical factors that moved the sensor from its desired location or damaged the hardware enough to prevent recording. Unknown failures resulted from signal loss not directly attributable to one of the other mechanisms [20]. Failure modes were designated for each experimental array according to this classification system.

3. Results

The impedance (IMP), amplitude (AMP), noise amplitude (Namp), SNR, and the number of VCs at early, middle and late recording sessions are given for each array in table 1. The trends in VC count, impedance, and failure mode over time are plotted in figure 3. Relevant clinical events, histologic findings, and assigned failure modes are included in table 1 as well. Results for all imaged arrays are presented in table 2. We focused the SEM analysis on important locations along the array, including the tips, shafts and bases of the electrodes along with the edges of the entire array. No significant difference was found between electrodes based on their spatial orientation within the array. The only exception was tissue density, which is discussed further in the following sections. The results for each array were as follows.

3.1. Control arrays

The control arrays were not placed *in vivo*, and were prepared as described earlier in the methods section.

Control arrays 1, 2, and 3 did not show any signs of platinum degradation, and only a few electrodes had minor parylene delamination at the platinum–parylene interface. The shafts and bases had some parylene irregularities, but did not have any cracks. These irregularities, or bumps, along the surface are normal findings and related to the manufacturing techniques used by BRMS. The edges did not have any silicone deposited, and there were no cracks in the parylene or silicon. Representative images from these arrays are shown in figure 4.

3.2. LN-LMSA

This array was placed in the left supplementary motor area and worked well until it was explanted at 37 days following euthanization. Failure was thus acute biological secondary to the death of the animal. Electrode impedances rose significantly over the first 2 weeks from a mean of 380 kOhm to 533 kOhm, and then started to fall by day 20 to 424 kOhm. There were 22 VCs with a mean PTP amplitude of 64 μV the day before explantation.

On SEM, the electrode tips of this array did not show evidence of platinum degradation or parylene delamination, but they were encapsulated by a thin film of tissue (~200–300 nm). The shafts showed uniform tissue growth with many fibroblasts and a few small cracks in the parylene. The base had many active macrophages and fibroblasts as well as a few cracks in the parylene. The edges did not have any silicone delamination, cracks, or tissue adhesions. See figure 5.

A thin layer of arachnoid was adherent to the array at the time of explantation (figure 2(a)). There was minimal undergrowth, but the capsule did appear to be continuous with both dura and arachnoid. Histology showed increased Iba1 activity throughout the implant site and mildly increased GFAP reactivity at the edges of the implant site. The NeuN stain did not penetrate the tissue well, but suggests a minor decrease in the neuronal population (figures 6(a)–(c)).

3.3. SCT-RV1

This array was placed in the right occipital lobe to record visual cortex (V1). It failed within the first week after implantation and was explanted at 99 days. Failure was classified as acute unknown but a mechanical failure of the connector was suspected. As a result, we were unable to gather any useful neural recordings.

On SEM, the tips did not show any platinum degradation or parylene delamination. There was a thin (~250 nm) partial tissue encapsulation present at the tips. Several of the shafts had longitudinal cracks in the parylene, tissue encapsulation was thin, and there were few cells. No collagen fibers were present. Along with many cells at the base, there were a few cracks in the parylene. The edges did not have any silicone delamination and cracks were rare. Few tissue adhesions were found on the silicone. See figure 7.

A dense fibrous capsule was found during the explant procedure with dura adhered to the top of the array. The undergrowth was slightly thinner compared to the tissue found underneath older arrays (figure 2(b)). Thin fibrous sheaths had grown around the electrodes, penetrating the cortex. These sheaths were continuous with the dural encapsulation and easily peeled away from the surrounding arachnoid (figure 2(c)). There is no histology for this animal, as it remains in good health.

3.4. GAR-RMI

This array was placed in the right primary motor cortex (RMI) and explanted at 554 days. The wire bundle was cut at the skull and the array was internalized at 119 days to prevent the sub-dural spread of a superficial wound infection. Mean impedance was only checked over the first week but shows the characteristic rise seen in other arrays, going from 470 kOhm pre-implant to 931 kOhm 8 days later. Seven days after implantation there were 61 VCs with a mean PTP amplitude of 79 μV. By day 39, the VC count was 64 with a mean PTP amplitude of 83 μV. Failure was classified as acute mechanical secondary to the wire bundle being cut at day 119.

SEM showed complete encapsulation of the tips with a ~250–500 nm tissue layer. The shafts were uniformly covered in a thin (~250 nm) sheath but also had numerous thick (~1–5 μm) tissue adhesions with many fibroblasts. Collagen fibers connecting adjacent electrodes were seen, and these fibers were more heavily concentrated in the center of the array as opposed to the periphery. Tissue invasion into parylene cracks was common throughout the array. The base had a few shallow cracks in the parylene, a few cells, and a thin (~250 nm) fibrous layer. The edges did not have any cracks, but did have some short segments of silicone delamination. A few tissue adhesions were found on the silicone. See figure 8.

Thick fibrous encapsulation tissue was found during explantation and was continuous with the dura. The tissue below this array was much softer than the usual capsule and appeared inflamed, however there was no purulence and tissue cultures were negative for infection. Much of this tissue was adherent to the array as well (figures 2(d)–(f)). There is no histology for this animal, as it remains in good health.

3.5. GAR-RPMv

This array was placed in the right ventral premotor area (RPMv) and explanted at 554 days. The wire bundle was cut at the skull and the array was internalized at 176 days to prevent the sub-dural spread of a superficial wound infection. Mean impedance was only checked over the first week but shows the characteristic rise seen in other arrays, going from 340 kOhm pre-implant to 898 kOhm 8 days later. Seven days after implantation there were 45 VCs with a mean PTP amplitude of 74 μV. By day 175, the VC count fell to 20 with a mean PTP amplitude of 55 μV. Failure was classified as acute mechanical secondary to the wire bundle being cut at day 176.

SEM showed complete encapsulation of the tips with a ~250–500 nm tissue layer. A few electrodes had cracked platinum tips. The shafts were uniformly covered in a thin (~250 nm) sheath but also had numerous thick (~1–5 μm) tissue adhesions with many fibroblasts. Collagen fibers connecting adjacent electrodes were seen, with tissue often invading the

many longitudinal and transverse cracks in the parylene. The base had many shallow cracks in the parylene with a few cells and a thin (~250 nm) fibrous layer. The edges did not have any cracks, but did have some minor silicone delamination and a few tissue adhesions on the silicone. See figure 9.

A dense fibrous capsule continuous with the dura was identified during the explant procedure (figures 2(g)–(i)). Thick fibrous sheaths had grown down into the cortex along the electrode tracts, similar to those seen in SCT-RVI. There is no histology for this animal, as it remains in good health.

3.6. LA-LMI4

This array was placed in the left primary motor cortex (LMI) and explanted at 639 days. Mean impedance at the time of implant was 214 kOhm. Impedances were not checked again until day 639 just prior to explant and the mean was 149 kOhm. Twenty-one days after implantation there were 37 VCs with a mean PTP amplitude of 94 μV. By day 99, the VC count went to 7 with a mean PTP amplitude of 60 μV. There were no VCs on day 639 but LFP was recorded. During explantation, the array was found completely encapsulated within the dura (figure 2(j)). There were no visible electrode tracts within the cortex. Failure was classified as chronic biological secondary to meningeal encapsulation and extrusion.

SEM showed complete encapsulation of the tips with a ~250–500 nm tissue layer. The platinum did not appear to be degraded, but there was abundant delamination at the platinum/parylene interface. The shafts had a thick (~500 nm), irregular tissue encapsulation with many scattered fibroblasts. Collagen fibers connecting adjacent electrodes were seen, and these fibers were more heavily concentrated in the center of the array as opposed to the periphery. Tissue invasion into parylene cracks was common throughout the array. It often looked as though the parylene was being peeled off of the underlying silicon by these tissue adhesions. The base had many deep cracks in the parylene, a few cells, and a thick (~500 nm–1 μm) fibrous layer. The edges had many cracks, and there was abundant silicone delamination. Many tissue adhesions were found on the silicone and within the delaminated segments. See figure 10.

Histology confirmed that the array was completely out of the cortex and encapsulated by meningeal tissue (figures 6(d)–(f)). GFAP staining showed a thick layer of gliosis over the cortical surface of the implant site and a clear disruption of the normal cortical architecture consistent with a glial scar. Iba1 activity overlying the implant site was mildly increased, but was most dense in the arachnoid and dura that had enveloped the array. There was dense Iba1 reactivity in the region of the cortical scar as well. The NeuN stain showed that were was a clear violation of the normal cortical architecture at the implant site, with significant neuronal loss. Neurons immediately adjacent to the implant site appeared viable. These histology results suggest that the array was completely extruded from the brain and then encapsulated in a fibrous scar continuous with both arachnoid and dura. The high Iba1 activity suggests that this was an ongoing process at the time of explant.

3.7. RUS-LPMv2

This array was placed in the left ventral premotor cortex (LPMv) replacing a prior implant. The initial array was in place for 9 months and was replaced with a new array in order to perform a different experiment. The new array was implanted into an area of fresh, healthy brain over 1 cm away from the prior implant site. RUS-LPMv2 worked well until explanted at 994 days. Mean impedance at the time of implant was 335 kOhm, rose to 855 kOhm by day 8 and then dropped slowly over time to 251 kOhm by day 976. Fifty days after implantation there were 53 VCs with a mean PTP amplitude of 101 μV. By day 990, the VC count fell to 18 with a mean PTP amplitude of 70 μV. The array was removed after 994 days in order to conduct experiments on a different part of the brain. Failure was classified as acute mechanical secondary to surgical removal of the array.

SEM was performed on this array without sputter coating in order to see if there were features obscured by the coating process. Imaging of the tips showed widespread erosion of the platinum, often with cracks and peeling that separated the platinum from the underlying silicon. There was minimal erosion of the exposed silicon and a few electrodes showed tissue growth between the platinum and silicon. The extent of degradation at the tips was highly variable. Approximately half of the electrodes showed at least some evidence of platinum erosion. There was very little parylene delamination as well, but this may have been obscured by encapsulation tissue. The extent of degradation at the tips was nearly uniform in this array. The thick tissue (~500 nm) that adhered to the tips sometimes had pieces of platinum stuck in it. This finding suggests that some of the platinum that peeled off of the silicon may have done so as a result of the array extraction process. The tissue may have adhered so strongly to the tips that when the array was lifted out of the brain, the platinum was sheared off. Along the shafts was a regular, thick (>500 nm) tissue encapsulation with few cells. There were rare cracks in the parylene and many collagen fibers that were found at both the center and periphery of the array. There were many cells on the base, with a thick (~500 nm–1 μm) fibrous layer and few visible cracks in the parylene. At the edges were a few small points of silicone delamination except for the edge where the wire bundle attached. This edge had an approximately 1 mm segment of delamination between the parylene coated base and the silicone coated wire bundle. There were no obvious cracks along the base. Many tissue adhesions were found on the silicone elastomer. See figure 11.

A thick fibrous scar continuous with the dura was found during explantation. The tissue below this array (RUSLPMv2) was thicker than in the other array (RUS-LPFv2) from the same monkey and it appeared as though part of the array had been lifted out of the brain (figure 2(k)). There is no histology for this animal, as it remains in good health.

3.8. RUS-LPFv2

This array was placed in the left ventral prefrontal cortex (LPFv) replacing a prior implant. The initial array was in place for 9 months and was replaced with a new array in order to perform a different experiment. The new array was implanted into an area of fresh, healthy brain over 1 cm away from the prior implant site. RUS-LPFv2 worked well until explanted at 994 days. Mean impedance at the time of implant was 500 kOhm, rose to 795 kOhm by

day 8 and then dropped slowly over time to 466 kOhm by day 990. Fifty-one days after implantation there were 61 VCs with a mean PTP amplitude of 93 μV. By day 990, the VC count fell to 50 with a mean PTP amplitude of 71 μV. The array was removed after 994 days in order to conduct experiments on a different part of the brain. Failure was classified as acute mechanical secondary to surgical removal of the array.

SEM was also performed on this array without sputter coating. Imaging of the tips showed erosion of the platinum, often with cracks and peeling that separated the platinum from silicon underneath. There was erosion of the underlying silicon and thick (>500 nm) tissue encapsulation with growth between the platinum and silicon. There was some parylene delamination as well, but this was mostly obscured by encapsulation tissue. The extent of degradation at the tips was not uniform. Approximately two-thirds of the electrodes had obvious violation of the platinum and there was no spatial pattern to the severity of these findings. The majority of electrode tips only showed minor signs of platinum erosion, and a few showed none at all. Along the shafts was a regular, thick (>500 nm) tissue encapsulation with few cells. There were rare cracks in the parylene and rare collagen fibers. There were many cells on the base, with a thick (~500 nm–1 μm) fibrous layer and few visible cracks in the parylene. Along the edges were a few points of silicone delamination and many tissue adhesions were found on the silicone elastomer. See figure 12.

A thick, fibrous, and well-vascularized scar continuous with the dura was found during the explantation of this array (figure 2(l)). There is no histology for this animal, as it remains in good health.

3.9. LA-LPE3

This array was placed in the left parietal cortex (LPE) and explanted after 1051 days. Mean impedance at the time of implant was 214 kOhm. It rose rapidly to 774 kOhm by day 14 and then dropped slowly over time to 106 kOhm by day 1051. Forty-one days after implantation there were 56 VCs with a mean PTP amplitude of 81 μV. By day 471, the VC count was 59 with a mean PTP amplitude of 53 μV. The amplitude continued to drop slowly over time and there were no VCs by day 1008. Failure was classified as chronic unknown with the underlying cause likely being a combination of material degradation and tissue encapsulation.

SEM showed complete encapsulation of the tips with a tissue layer of approximately 500 nm. The platinum appeared to have eroded at almost every electrode tip (>95% of electrodes), and many of these sites had tissue growth into the resulting gap between platinum and silicon. Erosion was evident on the underlying silicon to varying degrees. The findings in this array were more consistent with a chronic process as opposed to the suspected shearing phenomenon seen in RUS-LPMv2. Delamination at the platinum/parylene interface seemed minimal, but was difficult to assess because the tissue encapsulation was generally too thick. The shafts had a thick (~500 nm–1 μm), uniform tissue encapsulation with many fibroblasts towards the base. The sheath appeared thicker (~1 μm–5 μm) towards the base of each shaft, where the fibroblasts were clustered. Collagen fibers connecting adjacent electrodes were not seen in this array. Very few cracks were noted in the parylene but may have been obscured by the especially thick fibrous sheath. The base

had some shallow cracks in the parylene, but was covered in a fibrous layer that varied from 250 nm to several microns in thickness. There were many cells at the base that appeared to be a mix of fibroblasts and macrophages. The edges had a few cracks and there was minimal evidence of silicone delamination. Many tissue adhesions were found on the silicone. See figure 13.

Dense encapsulation tissue had grown over the top as well as underneath this array. The tips of the electrodes were still partially within the cortex, although they were very superficial (figures 2(m)–(o)). Histology confirmed that the array was almost completely out of the cortex and wrapped in meningeal tissue (figures 6(g)–(i)). GFAP staining showed a thick layer of gliosis throughout the implant site and partial electrode tracts are clearly identified. Iba1 activity overlying the implant site was mildly increased, but the arachnoid/dura that had enveloped the array stained heavily. There was dense Iba1 reactivity in a region of the implant site where GFAP staining was most dense as well. The NeuN stain showed that neurons at the implant site were generally well preserved, although the cortical layers were notably compressed. There was a small area within the implant site where NeuN did not stain. This area coincides with the high GFAP and Iba1 staining and likely reflects focal damage to those neurons. Neurons immediately adjacent to the implant site appeared viable. These histology results suggest that the array was partially extruded from the brain while being encapsulated in a fibrous scar composed of meningeal cells. The high Iba1 activity suggests that this was an ongoing process at the time of explant.

4. Discussion

Research efforts investigating neuroprosthetic devices continue to focus on creating systems that can be clinically implemented with the potential to restore lost function to people with disabilities. Successful long-term clinical application of these devices depends upon intracortical MEAs that can be implanted without facing the currently inevitable prospect of signal attenuation.

The purpose of this study was to investigate the factors contributing to progressive signal decline by using SEM to visualize structural changes in chronically implanted arrays and histology to examine the tissue response at corresponding implant sites.

4.1. Biological failures

4.1.1. Gliosis—Numerous studies have attempted to address the biological responses leading to MEA failure. They have largely focused on the foreign body reaction, gliosis, neuronal death, and violation of the blood–brain barrier. Glial scar formation is typically complete within 6–12 weeks [40] and is most dense within 50–100 μm of the electrode tract, although more sensitive techniques have shown that GFAP reactivity is detectable up to 500 μm from the implant site [29, 41, 42]. Our histologic findings support these results.

Gliosis has been proposed to insulate the electrode from nearby neurons, hindering diffusion and increasing impedance [30, 40, 43]. The rapid rise in 1 kHz impedance seen in all of our arrays over the first 2 weeks has been observed in numerous other *in vivo* studies [21, 44–47]. One *in vitro* study reported that similar microelectrodes coated in astrocytes have an

impedance increase of about 270 kOhm but those coated with a combination of astrocytes and fibroblasts showed an increase of 540 kOhm [48]. This second number fits our data almost perfectly, suggesting that the early impedance changes we observed are due to gliosis as well as meningeal fibrosis.

Others claim that the gliotic scar also extends the distance between the electrode and its nearest target neurons and creates an inhibitory environment for neurite extension, repelling regenerating neural processes away from the recording sites [38, 49, 50]. This is thought to reduce recording quality as the maximum recordable distance is generally thought to be about 100 μm [17, 51, 52]. Several studies have shown that there is a graded loss of neuronal density that is most distinct in the first 50 μm from the implant site [27–29]. Potter-Baker also showed partial recovery of neuronal densities from 2 to 16 weeks post implant. The limited histology that we present here shows moderate gliosis at 1051 days but neuronal density appears grossly normal except for one small region as described in the results.

In sum, a glial scar clearly forms in response to MEA implants over 6–12 weeks and extends roughly 100 μm from the implant site where neuronal density may be slightly diminished but recovers with time. Our neural recordings show an early rise in impedance that is at least partially due to gliosis, but quality recordings are routinely obtained past 12 weeks suggesting that gliosis and neuronal cell death do not play a significant role in chronic electrode failures. The long-term drop in impedance is also inconsistent with gliosis as a chronic failure mode.

4.1.2. Meningeal encapsulation—Fibrous tissue encapsulation, however, may be a major factor contributing to chronic electrode failure. Progressive meningeal growth that gradually lifts the array out of the cortex could easily explain some of the observed signal loss [20, 36]. Fibrous electrode encapsulation has been reported in the literature as early as 1957 by Collias and Manuelidis [33]. Meningeal fibroblasts, which stain for vimentin, but not for GFAP, may migrate down the electrode shaft from the brain surface [53]. Kim *et al* (2004) found a thin layer (1 to 2 cells) of GFAP negative but vimentin positive cells surrounding implants that were in contact with the meninges [35]. The authors concluded that meningeal fibroblasts had migrated down the probe from the top of the cortex. Shearer and Fawcett have also demonstrated that meningeal fibroblasts migrate into a lesion cavity, forming a fibrotic scar and ‘accessory’ glia limitans [37]. They conclude that this infiltration reestablishes the meningeal layer that normally surrounds the brain, and thus restores the intraparenchymal and extraparenchymal boundary. This process would explain the dense white fibrous tissue found underneath our arrays that tracts along the wire bundle, dove down into the cortex, and was continuous with both arachnoid and dura. Our histology (figure 6) also showed that this tissue was GFAP negative. Future studies by our group will likely confirm that fibrous encapsulation material stains for vimentin.

Fibroblasts from the dural border cells that line the inner surface of the dura within the subdural space are well known to be the origin of subdural membranes in patients with chronic subdural hematomas [54]. Other research has shown that fibroblasts have an increased ability to attach and spread along flat, ionized parylene-C surfaces in the presence of serum proteins [34]. We propose that dural border cells grow along the implant seeking to

re-establish the normal layered architecture of the meninges. These dural fibroblasts are likely the same cells seen with SEM on the base of our arrays, producing a fibrous sheath along the electrode shafts. This sheath was noted to vary from ~250 nm to 5 μm, consistent with the laminar structure of dura. Several SEM studies of normal human dura have shown that it ranges from 300 to 800 μm in thickness and is composed of ~80 laminae that are each 4–5 μm thick. These individual laminae are composed of ~8–12 sub-laminae of fine collagen fibers that range from 200 to 600 nm in thickness. Larger elastic collagen fibers (~2 μm) are often found within this matrix [55–58]. Our SEM findings suggest that dural sub-laminae remain adherent to the arrays and as the encapsulation matures; the tissue adhesions contain an increasing number of sub-laminae. Several of our arrays also clearly demonstrated the presence of elastic collagen fibers. As discussed earlier, the rise in impedance over the first 2 weeks likely reflects the initial recruitment of astrocytes and fibroblasts with early deposition of the fibrous encapsulation. Thus, our findings are consistent with typical dural architecture. The compact (~2–5 μm) fibroblastic layer observed within electrode tracts by Schmidt in 1993 also looks like a dural laminae [41]. Similarly, in 1998 Rousche and Normann showed a comparable fibrous tract extending into the cortex of cats implanted with the same type of array used in this study [36]. It is often difficult to discern the exact boundary between dura and arachnoid when examining the encapsulation tissue surrounding long-term arrays. Ultimately, the tissue encapsulating our MEAs is composed of fine collagen produced by fibroblasts that originate in the subdural space, probably from the dural border cell layer. This biologic reaction is clearly a significant barrier to long-term recording success and a major factor in chronic electrode failure. This process could easily account for the progressive decline in signal amplitudes as electrodes are withdrawn from the brain by fibrotic encapsulation tissue. It does not, however, explain the progressive decline in impedances and noise amplitudes. These observations are most likely due to concomitant material failures.

4.2. Material failures

4.2.1. Electrode corrosion—The extent to which metal electrodes used for neuroprosthetics degrade over time is a major concern. Tungsten electrodes have demonstrated extensive corrosion both *in vitro* and *in vivo*. Prasad *et al* in 2012 presented SEM of tungsten electrode corrosion after 9 months in rat cortex [21]. While Tungsten may lack the necessary durability for neuroprosthetic applications, platinum is generally thought to be sufficiently inert. In a 1985 human study, Donaldson examined a platinum stimulating electrode used as a cortical visual prosthetic that was *in vivo* for 7 months and showed no obvious signs of corrosion on SEM [59]. In 1990, Shepard looked at SEM of cochlear implants (also stimulating electrodes) explanted after 1000 days and found no definitive signs of corrosion [60]. For comparison, these large electrodes were 50 μm thick, whereas the platinum on our arrays is only 500 nm thick. Contrary to these findings, Bernstein found in 1977 that platinum stimulating electrodes corrode more severely *in vivo* than *in vitro* with stimulation, and concluded that platinum should not be used for neuroprosthetics, although they suggest that platinum recording electrodes should be fine.

It is well known that platinum is susceptible to oxidation–reduction reactions and corrosion, however the conditions under which this occurs are generally much more extreme than those

found within the brain [61–65]. Nonetheless, efforts have been made to define the safe stimulation parameters needed to avoid this electrochemical corrosion effect [66, 67]. One study in cats found evidence of platinum dissolution up to 1 mm from the electrode with varying degrees of stimulation [68]. Others have found that platinum corrosion is accelerated by the presence of Cl^- ions [64], but inhibited when the platinum electrode is coated with a protein film [69]. Donaldson also conducted *in vitro* tests with platinum stimulating electrodes in saline solution and albumin solution showing less platinum degradation with the protein solution [59]. In 2009, Gencolgu *et al* found that stimulated platinum corrodes in a variety of buffered solutions. The authors concluded that 'despite its well known resistance to corrosion, platinum is susceptible to a range of morphological and chemical changes which can potentially alter performance of medical microdevice electrodes over time ...' [70].

Despite this body of literature on platinum corrosion, few conclusions can be extended to the electrodes used in this study. Our electrodes were not stimulated, except for the occasional impedance check, and were likely not subjected to the extreme acid–base environments under which platinum typically oxidizes. The lack of long-term *in vivo* analysis on comparable platinum recording electrodes also limits comparisons to our findings.

We found the platinum on our electrodes to be grossly intact on all arrays from day 37 to day 639. The arrays from day 994 to day 1051, however, showed many electrodes with clear signs of platinum corrosion. This may, in some instances, be due to a mechanical shearing effect as described in the results. It is also possible that pitting corrosion is taking place at the tips, weakening the platinum film and making it more susceptible to tissue invasion and mechanical disruption. We suspect that a very slow oxidation of platinum is taking place. The reactive oxygen species (OH, NO, O_2-, H_2O_2) that are produced by immune cells during the foreign body reaction are excellent reagents for the oxidation of platinum. The rate is likely so slow because of the relatively low concentration of these molecules and the lack of sufficient over-potential current. Relatively speaking, sputtered platinum–iridium layers may be advantageous over the sputtered platinum thin film utilized in this study. As material for stimulation electrodes, platinum–iridium demonstrates increased hardness, corrosion stability, and enhanced charge injection capacity as compared to pure platinum [71, 72]. Future studies need to quantify the extent to which metal electrodes participate in oxidation–reduction reactions *in vivo* over several years.

4.2.2. Parylene degradation—Parylene-C is generally considered to be a biocompatible insulation material for neuroprosthetic sensors [73]. There is little data, however, on how parylene-C performs after several years *in vivo*. In 1977 Loeb *et al* demonstrated parylene degradation after 275 days in monkey motor cortex. The authors documented a progressive drop in impedance and 'gaping cracks' were seen with SEM. They also suggested that cracks and loss of tensile strength allow macrophages to break up the parylene *in vivo* [74]. Schmidt documented similar findings in 1988 when he found craters and longitudinal cracks in parylene coated electrodes after 1144 days in monkeys. These electrodes displayed a progressive drop in impedances as well. The author suggested that surface irregularities and dust contamination might weaken sections of the insulation and predispose to failure [16]. Our findings are consistent with both of these studies. We had a progressive decline in

impedances and found numerous cracks in our multi-year arrays. The cracks appeared to be more common near surface irregularities and tissue invasion into cracks and delaminated segments near the tips were also observed in several of our arrays. It is also worth noting that our control arrays did not show any evidence of cracking, demonstrating that the preservation process used in this study was not responsible.

Recent *in vitro* work has shown that heat-treated parylene is a better water barrier and less likely to delaminate but has an increased crystallinity, which may make the polymer more likely to crack [75, 76]. Exposure of parylene-C to artificial blood plasma and cerebrospinal fluid for 2 months has also been shown to increase the crystallinity of the polymer, making it more brittle. Body fluids in contact with parylene may also lead to the recruitment of inflammatory or fibrogenic agents [77]. The notion that parylene-C is a suitable, biocompatible material for long-term neuroprosthetics no longer seems valid. While it may be one of the best polymers currently available, it is not sufficient for chronic applications. Further efforts must be made to find a more durable insulation material, one that will last for many years *in vivo*.

4.3. Mechanical failures

Mechanical failure modes were not clearly observed in this study. The missing platinum at the tips of some electrodes appeared to have been sheared or peeled off, but there is no way to be certain. If shearing did occur, however, it is likely to be an artifact of the extraction process itself and not actually a failure mode. The only other possible mechanical failure that we observed was related to silicone delamination. The segments of silicone that had peeled away from the array near the base of the wire bundle may have been stressed at the junction. The triangular base of the wire bundle is often held with forceps during surgery in order to position the array while protecting the electrodes tips. This part of the array may therefore be under additional stress making it easier for the silicone to peel off of the parylene-coated base.

5. Conclusions

Neuroprosthetic devices have enormous potential to improve the lives of disabled people. The possible clinical applications are vast and have only just begun to be explored. However, routine clinical use of intracortical neuroprosthetics has not yet occurred. This is primarily due to the fact that sensors fail over time. There is no single explanation for why intracortical MEAs fail over time. Failures result from a combination of biological, material, and mechanical factors. SEM has shown us that platinum and parylene degrade over time in a predictable fashion. Future design efforts must focus on finding more durable materials that will prolong the functional life of intracortical neuroprosthetic sensors. SEM has also provided us with further insight into the structure and significance of meningeal tissue encapsulation. We need to focus research on the fundamental cellular mechanisms of meningeal fibrosis so that we can develop drugs or materials capable of controlling this process. In order for intracortical neuroprosthetic devices to be adopted into routine clinical use they must provide consistent high-quality neural signals for at least a decade. With improved insulation materials, more durable alloys for electrode tips, and pharmacologic

suppression of fibrosis and gliosis, neuroprosthetics will become a powerful tool in the routine treatment of disabled patients.

Acknowledgments

The authors would like to thank Corey Triebwasser for his help with preparing the specimens and Mike Greunhagen of Blackrock Microsystems for his generous donation of the control arrays used in this study.

References

1. Hochberg LR, Donoghue JP. Sensors for brain–computer interfaces. IEEE Eng. Med. Biol. Mag. 2006; 25:32–8. [PubMed: 17020197]
2. Hochberg LR, Serruya MD, Friehs GM, Mukand JA, Saleh M, Caplan AH, Branner A, Chen D, Penn RD, Donoghue JP. Neuronal ensemble control of prosthetic devices by a human with tetraplegia. Nature. 2006; 442:164–71. [PubMed: 16838014]
3. Donoghue JP. Connecting cortex to machines: recent advances in brain interfaces. Nat. Neurosci. 2002; 5:1085–8. [PubMed: 12403992]
4. Donoghue JP, Nurmikko A, Black M, Hochberg LR. Assistive technology and robotic control using motor cortex ensemble-based neural interface systems in humans with tetraplegia. J. Physiol. 2007; 579:603–11. [PubMed: 17272345]
5. Kim S-P, Simeral JD, Hochberg LR, Donoghue JP, Black MJ. Neural control of computer cursor velocity by decoding motor cortical spiking activity in humans with tetraplegia. J. Neural. Eng. 2008; 5:455–76. [PubMed: 19015583]
6. Chapin JK, Moxon KA, Markowitz RS, Nicolelis MA. Real-time control of a robot arm using simultaneously recorded neurons in the motor cortex. Nat. Neurosci. 1999; 2:664–70. [PubMed: 10404201]
7. Hochberg LR, et al. Reach and grasp by people with tetraplegia using a neurally controlled robotic arm. Nature. 2013; 485:372–5. [PubMed: 22596161]
8. Collinger JL, Wodlinger B, Downey JE, Wang W, Tyler-Kabara EC, Weber DJ, McMorland AJ, Velliste M, Boninger ML, Schwartz AB. High-performance neuroprosthetic control by an individual with tetraplegia. Lancet. 2013; 381:557–64. [PubMed: 23253623]
9. Gilja V, Nuyujukian P, Chestek CA, Cunningham JP, Yu BM, Fan JM, Ryu SI, Shenoy KV. A brain machine interface control algorithm designed from a feedback control perspective. Conf. Proc. IEEE Engineering in Medicine Biology Society. 2012; 2012:1318–22.
10. Nuyujukian P, Fan JM, Kao JC, Ryu SI, Shenoy KV. A high-performance keyboard neural prosthesis enabled by task optimization. IEEE Trans. Biomed. Eng. 2014; 1
11. Mioche L, Singer W. Long-term recordings and receptive field measurements from single units of the visual cortex of awake unrestrained kittens. J. Neurosci. Methods. 1988; 26:83–94. [PubMed: 3199850]
12. Liu X, McCreery DB, Carter RR, Bullara LA, Yuen TG, Agnew WF. Stability of the interface between neural tissue and chronically implanted intracortical microelectrodes. IEEE Trans. Rehabil. Eng. 1999; 7:315–26. [PubMed: 10498377]
13. Chestek CA, et al. Long-term stability of neural prosthetic control signals from silicon cortical arrays in rhesus macaque motor cortex. J. Neural Eng. 2011; 8:045005. [PubMed: 21775782]
14. Fontani G. A technique for long term recording from single neurons in unrestrained behaving animals. Physiol. Behav. 1981; 26:331–3. [PubMed: 7232539]
15. Krüger J, Caruana F, Volta RD, Rizzolatti G. Seven years of recording from monkey cortex with a chronically implanted multiple microelectrode. Front. Neuroeng. 2010; 3:6. [PubMed: 20577628]
16. Schmidt EM, Mcintosh JS, Bak MJ. Long-term implants of Parylene-C coated microelectrodes. Med. Biol. Eng. Comput. 1988; 26:96–101. [PubMed: 3199908]
17. Drake KL, Wise KD, Farraye J, Anderson DJ, BeMent SL. Performance of planar multisite microprobes in recording extracellular single-unit intracortical activity. IEEE Trans. Biomed. Eng. 1988; 35:719–32. [PubMed: 3169824]

18. Palmer C. A microwire technique for long term recording of single units in the brains of unrestrained animals [proceedings]. J. Physiol. 1976; 263:99P–01P.
19. Burns BD, Stean JP, Webb AC. Recording for several days from single cortical neurons in completely unrestrained cats. Electroencephalogr. Clin. Neurophysiol. 1974; 36:314–8. [PubMed: 4130612]
20. Barrese JC, Rao N, Paroo K, Triebwasser C, Vargas-Irwin C, Franquemont L, Donoghue JP. Failure mode analysis of silicon-based intracortical microelectrode arrays in non-human primates. J. Neural Eng. 2013; 10:066014. [PubMed: 24216311]
21. Prasad A, Xue Q-S, Sankar V, Nishida T, Shaw G, Streit WJ, Sanchez JC. Comprehensive characterization and failure modes of tungsten microwire arrays in chronic neural implants. J. Neural Eng. 2012; 9:056015. [PubMed: 23010756]
22. Kipke DR, Vetter RJ, Williams JC, Hetke JF. Silicon-substrate intracortical microelectrode arrays for long-term recording of neuronal spike activity in cerebral cortex. IEEE Trans. Neural Syst. Rehabil. Eng. 2003; 11:151–5. [PubMed: 12899260]
23. Suner S, Fellows MR, Vargas-Irwin C, Nakata GK, Donoghue JP. Reliability of signals from a chronically implanted, silicon-based electrode array in non-human primate primary motor cortex. IEEE Trans. Neural Syst. Rehabil. Eng. 2005; 13:524–41. [PubMed: 16425835]
24. Jorfi M, Skousen JL, Weder C, Capadona JR. Progress towards biocompatible intracortical microelectrodes for neural interfacing applications. J. Neural Eng. 2014; 12:1–45.
25. Polikov VS, Tresco PA, Reichert WM. Response of brain tissue to chronically implanted neural electrodes. J. Neurosci. Methods. 2005; 148:1–18. [PubMed: 16198003]
26. Winslow BD, Christensen MB, Yang W-K, Solzbacher F, Tresco PA. A comparison of the tissue response to chronically implanted Parylene-C-coated and uncoated planar silicon microelectrode arrays in rat cortex. Biomaterials. 2010; 31:9163–72. [PubMed: 20561678]
27. Biran R, Martin DC, Tresco PA. Neuronal cell loss accompanies the brain tissue response to chronically implanted silicon microelectrode arrays. Exp. Neurology. 2005; 195:115–26.
28. Biran R, Martin DC, Tresco PA. The brain tissue response to implanted silicon microelectrode arrays is increased when the device is tethered to the skull. J. Biomed. Mater. Res. A. 2007; 82:169–78. [PubMed: 17266019]
29. Potter-Baker KA, et al. A comparison of neuroinflammation to implanted microelectrodes in rat and mouse models. Biomaterials. 2014; 35:5637–46. [PubMed: 24755527]
30. Schultz RL, Willey TJ. The ultrastructure of the sheath around chronically implanted electrodes in brain. J. Neurocytol. 1976; 5:621–42. [PubMed: 1003257]
31. Griffith RW, Humphrey DR. Long-term gliosis around chronically implanted platinum electrodes in the Rhesus macaque motor cortex. Neurosci. Lett. 2006; 406:81–6. [PubMed: 16905255]
32. Marin C, Fernandez E. Biocompatibility of intracortical microelectrodes: current status and future prospects. Front. Neuroeng. 2010; 3:8. [PubMed: 20577634]
33. Collias JC, Manuelidis EE. Histopathological changes produced by implanted electrodes in cat brains; comparison with histopathological changes in human and experimental puncture wounds. J. Neurosurgery. 1957; 14:302–28.
34. Wei L, Lakhtakia A, Roopnariane AP, Ritty TM. Human fibroblast attachment on fibrous parylene-C thin-film substrates. Mater. Sci. Eng. C. 2010; 30:1252–9.
35. Kim Y-T, Hitchcock RW, Bridge MJ, Tresco PA. Chronic response of adult rat brain tissue to implants anchored to the skull. Biomaterials. 2004; 25:2229–37. [PubMed: 14741588]
36. Rousche PJ, Normann RA. Chronic recording capability of the Utah Intracortical Electrode Array in cat sensory cortex. J. Neurosci. Methods. 1998; 82:1–15. [PubMed: 10223510]
37. Shearer MC, Fawcett JW. The astrocyte/meningeal cell interface—a barrier to successful nerve regeneration? Cell Tissue Res. 2001; 305:267–73. [PubMed: 11545264]
38. Fawcett JW, Asher RA. The glial scar and central nervous system repair. Brain Res. Bull. 1999; 49:377–91. [PubMed: 10483914]
39. Rousche PJ, Normann RA. A method for pneumatically inserting an array of penetrating electrodes into cortical tissue. Ann. Biomed. Eng. 1992; 20:413–22. [PubMed: 1510293]

40. Turner JN, Shain W, Szarowski DH, Andersen M, Martins S, Isaacson M, Craighead H. Cerebral astrocyte response to micromachined silicon implants. Exp. Neurology. 1999; 156:33–49.
41. Schmidt S, Horch K, Normann R. Biocompatibility of silicon-based electrode arrays implanted in feline cortical tissue. J. Biomed. Mater. Res. 1993; 27:1393–9. [PubMed: 8263001]
42. Thelin J, Jörntell H, Psouni E, Garwicz M, Schouenborg J, Danielsen N, Linsmeier CE. Implant size and fixation mode strongly influence tissue reactions in the CNS. PLoS One. 2011; 6:e16267. [PubMed: 21298109]
43. Roitbak T, Syková E. Diffusion barriers evoked in the rat cortex by reactive astrogliosis. Glia. 1999; 28:40–8. [PubMed: 10498821]
44. Williams JC, Hippensteel JA, Dilgen J, Shain W, Kipke DR. Complex impedance spectroscopy for monitoring tissue responses to inserted neural implants. J. Neural. Eng. 2007; 4:410–23. [PubMed: 18057508]
45. Prasad A, Sanchez JC. Quantifying long-term microelectrode array functionality using chronic *in vivo* impedance testing. J. Neural Eng. 2012; 9:026028. [PubMed: 22442134]
46. Vetter RJ, Williams JC, Hetke JF, Nunamaker EA, Kipke DR. Chronic neural recording using silicon-substrate microelectrode arrays implanted in cerebral cortex. IEEE Trans. Biomed. Eng. 2004; 51:896–904. [PubMed: 15188856]
47. Mercanzini A, Colin P, Bensadoun J-C, Bertsch A, Renaud P. *In vivo* electrical impedance spectroscopy of tissue reaction to microelectrode arrays. IEEE Trans. Biomed. Eng. 2009; 56:1909–18. [PubMed: 19362904]
48. Merrill DR, Tresco PA. Impedance characterization of microarray recording electrodes *in vitro*. IEEE Trans. Biomed. Eng. 2005; 52:1960–5. [PubMed: 16285400]
49. Stichel CC, Muller HW. The CNS lesion scar: new vistas on an old regeneration barrier. Cell Tissue Res. 1998; 294:1–9. [PubMed: 9724451]
50. Bovolenta P, Fernaud-Espinosa I. Nervous system proteoglycans as modulators of neurite outgrowth. Prog. Neurobiol. 2000; 61:113–32. [PubMed: 10704995]
51. Henze DA, Borhegyi Z, Csicsvari J, Mamiya A, Harris KD, Buzsaki G. Intracellular features predicted by extracellular recordings in the hippocampus *in vivo*. J. Neurophysiol. 2000; 84:390–400. [PubMed: 10899213]
52. Buzsáki G. Large-scale recording of neuronal ensembles. Nat. Neurosci. 2004; 7:446–51. [PubMed: 15114356]
53. Cui X, Wiler J, Dzaman M, Altschuler RA, Martin DC. *In vivo* studies of polypyrrole/peptide coated neural probes. Biomaterials. 2003; 24:777–87. [PubMed: 12485796]
54. Friede RL, Schachenmayr W. The origin of subdural neomembranes: II. Fine structural of neomembranes. Am. J. Pathol. 1978; 92:69–84. [PubMed: 686149]
55. Reina MA, López-García A, Dittmann M, De Andrés JA. Analysis of the external and internal surface of human dura mater with scanning electron microscopys. Rev. Esp. Anestesiol. Reanim. 1996; 43:130–4. [PubMed: 8815465]
56. Reina M, Dittmann M, Garcia A, Vanzundert A. New perspectives in the microscopic structure of human dura mater in the dorsolumbar region. Reg. Anesthesia Pain Med. 1997; 22:161–6.
57. Dittmann M, Reina MAM, García AL. New results in the visualization of the spinal dura mater with scanning electron microscopy. Anaesthesist. 1998; 47:409–13. [PubMed: 9645282]
58. Bashkatov AN, Genina EA, Sinichkin YP, Kochubey VI, Lakodina NA, Tuchin V. Glucose and mannitol diffusion in human dura mater. Biophys. J. 2003; 85:3310–8. [PubMed: 14581232]
59. Donaldson PE, Donaldson ND, Brindley GS. Life of Pt and Pt–Ir stimulating electrodes in neurological prostheses. Med. Biol. Eng. Comput. 1985; 23:84–6. [PubMed: 3974326]
60. Shepherd BK, Clark GM. Scanning electron microscopy of platinum scala tympani electrodes following chronic stimulation in patients. Biomaterials. 1991; 12:417–23. [PubMed: 1888811]
61. Wang JX, Markovic NM, Adzic R. Kinetic analysis of oxygen reduction on Pt(111) in acid solutions: intrinsic kinetic parameters and anion adsorption effects. J. Phys. Chem. B. 2004; 108:4127–33.

62. Cogan SF, Ehrlich J, Plante TD, Gingerich MD, Shire DB. Contribution of oxygen reduction to charge injection on platinum and sputtered iridium oxide neural stimulation electrodes. IEEE Trans. Biomed. Eng. 57:2313–21. [PubMed: 20515708]

63. Kodera F, Kuwahara Y, Nakazawa A, Umeda M. Electrochemical corrosion of platinum electrode in concentrated sulfuric acid. J. Power Sources. 2007; 172:698–703.

64. Llopis J, Sancho A. Electrochemical corrosion of platinum in hydrochloric acid solutions. J. Electrochem. Soc. 1961; 108:720–6.

65. Katsounaros I, Schneider WB, Meier JC, Benedikt U, Biedermann PU, Auer A, Mayrhofer KJ. Hydrogen peroxide electrochemistry on platinum: towards understanding the oxygen reduction reaction mechanism. Phys. Chem. Chem. Phys. 2012; 14:7384–91. [PubMed: 22517633]

66. Brummer SB, McHardy J, Turner MJ. Electrical stimulation with Pt electrodes: trace analysis for dissolved platinum and other dissolved electrochemical products. Brain Behav. Evol. 1977; 14:10–22. [PubMed: 13907]

67. McHardy J, Robblee LS, Marston JM, Brummer SB. Electrical stimulation with Pt electrodes: IV. Factors influencing Pt dissolution in inorganic saline. Biomaterials. 1980 (doi: 10.1016/0142-9612(80)90034-4).

68. Robblee LS, McHardy J, Agnew WF, Bullara LA. Electrical stimulation with Pt electrodes: VII. Dissolution of Pt electrodes during electrical stimulation of the cat cerebral cortex. J. Neurosci. Methods. 1983; 9:301–8. [PubMed: 6668956]

69. Robblee LS, McHardy J, Marston JM, Brummer SB. Electrical stimulation with Pt electrodes: V. The effect of protein on Pt dissolution. Biomaterials. 1980; 1:135–9. [PubMed: 7470564]

70. Gencoglu A, Minerick A. Chemical and morphological changes on platinum microelectrode surfaces in AC and DC fields with biological buffer solutions. Lab Chip. 2009; 9:1866–73. [PubMed: 19532961]

71. Darling AS. Iridium platinum alloys—a critical review of their constitution and properties. Platinum Met. Rev. 1960; 4:18–26.

72. Negi S, Bhandari R, Rieth L, Van Wagenen R, Solzbacher F. Neural electrode degradation from continuous electrical stimulation: comparison of sputtered and activated iridium oxide. J. Neurosci. Methods. 2010; 186:8–17. [PubMed: 19878693]

73. Stark N. Literature review: biological safety of parylene C. Med. Plast. Biomater. 1996

74. Loeb GE, Bak MJ, Salcman M, Schmidt EM. Parylene as a chronically stable, reproducible microelectrode insulator. IEEE Trans. Biomed. Eng. 1977; BME-24:121–8. [PubMed: 408260]

75. Seymour JP, Elkasabi YM, Chen H-Y, Lahann J, Kipke DR. The insulation performance of reactive parylene films in implantable electronic devices. Biomaterials. 2009; 30:6158–67. [PubMed: 19703712]

76. Davis, Benetatos, Regnault, WineyElabd. The influence of thermal history on structure and water transport in Parylene C coatings. Polymer. 2011; 52:9.

77. Beshchasna N, Adolphi B, Granovsky S, Braunschweig M, Schneider W, Uhlemann J, Wolter K-J. Influence of artificial body fluids and medical sterilization procedures on chemical stability of Parylene C. Electronic Components and Technology Conf. Proc. 2010:1846–52.

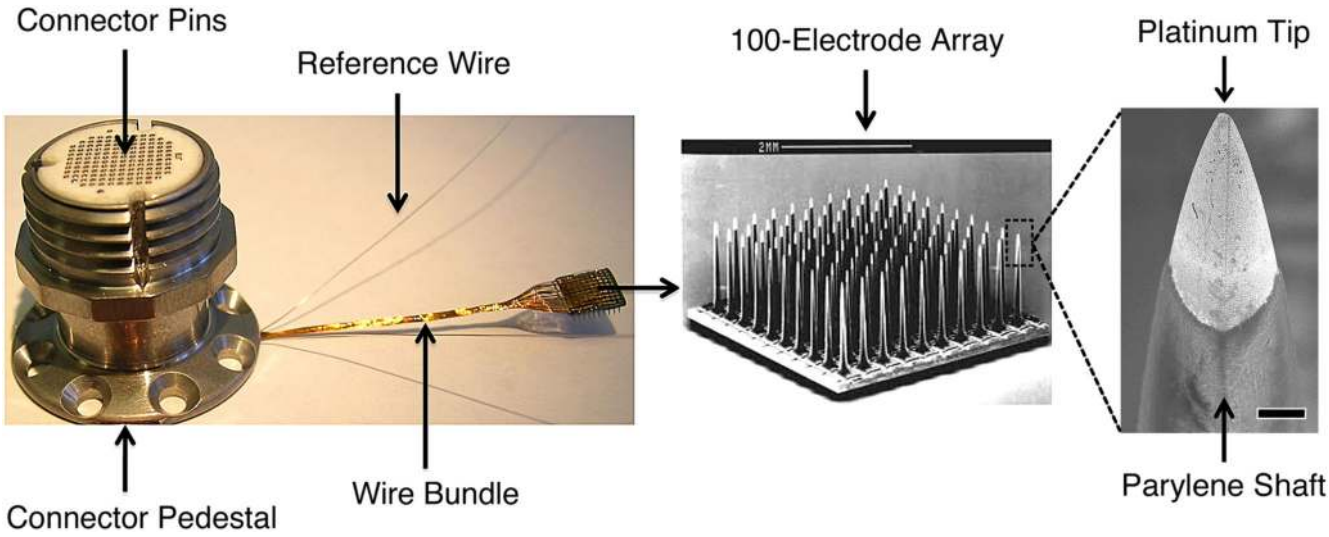

Figure 1.

Blackrock Microsystem's silicon-based MEA. *Left*: skull-mounted titanium pedestal showing orientation of wire bundle and subdural reference electrodes. *Middle*: SEM of the 100-microelectrode array, scale bar is 2 mm. *Right*: SEM of a single electrode tip highlighting the platinum-coated silicon tip and parylene-coated silicon shaft, scale bar is 10 μm.

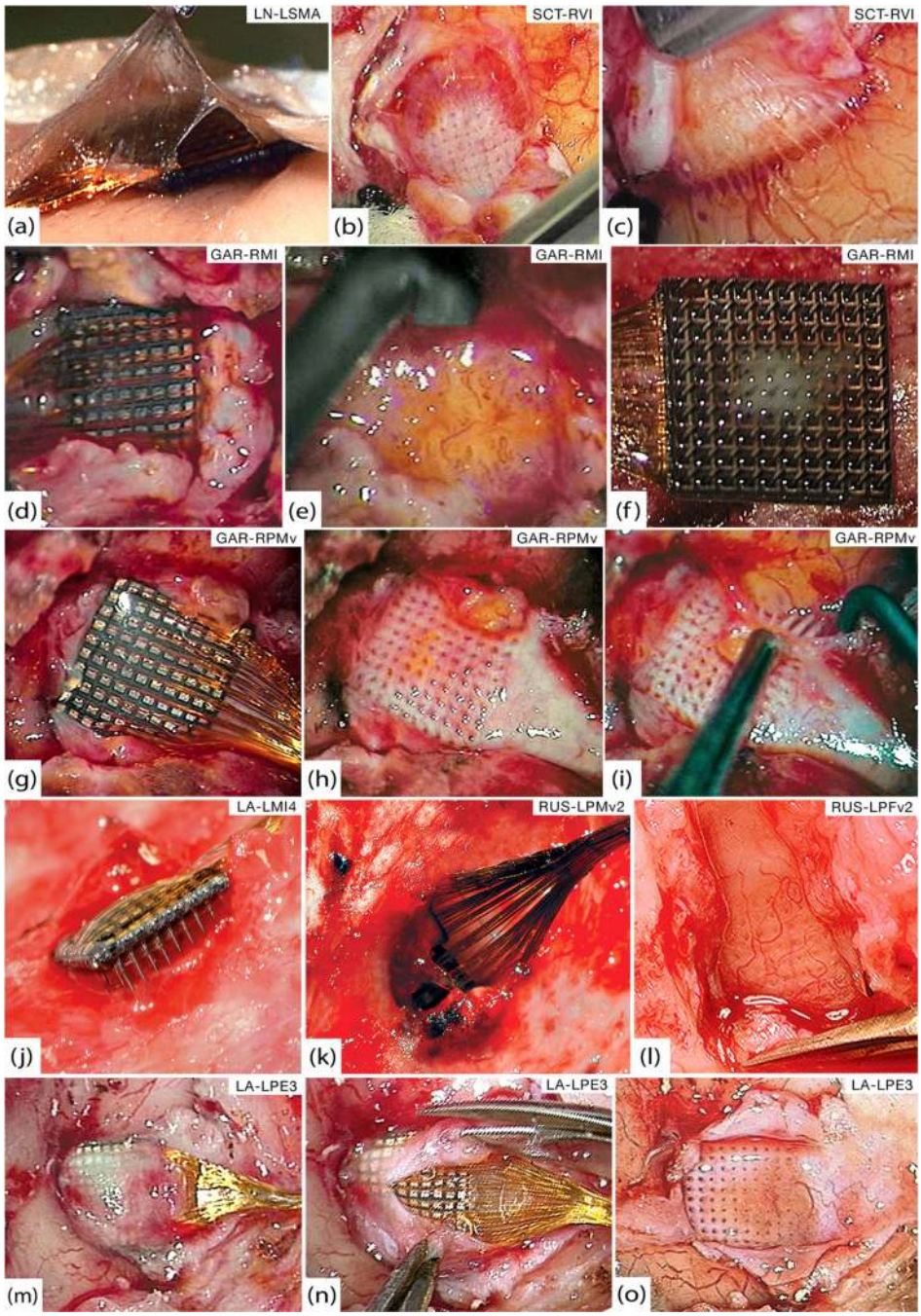

Figure 2.

Gross pathology. (a) Thin encapsulation tissue of LN-LSMA at 37 days that appears continuous with both arachnoid and dura. (b) Bed of encapsulation tissue underneath SCT-RVI at 99 days. (c) Fibrous sheaths around electrode tracts penetrating the cortex from the below tissue seen in (b). (d) GAR-RMI *in vivo* at 554 days after overlying dura has been cut away. (e) Friable, inflamed tissue underneath GAR-RMI (f) Tissue adherent to the underside of GAR-RMI. (g) GAR-RPMv *in vivo* at 554 days after opening dural capsule. (h) Thick bed of encapsulation tissue underneath GAR-RPMv. (i) Thick fibrous sheaths around

electrode tracts were seen diving down into the cortex as the tissue bed from (h) was reflected. (j) At 639 days, LA-LMI4 was completely encapsulated by dura and much of the array was extradural. (k) RUS-LPMv2 was entirely wrapped in dura and partially extruded from the cortex at 994 days. (l) Highly-vascularized bed of thick encapsulation tissue continuous with the dura found below RUS-LPFv2 at 994 days. (m) LA-LPE3 *in vivo* at 1051 days. The cut edges of the dura are visible on either side of the wire bundle and encapsulation tissue covers the array. (n) Microsurgical dissection of the capsule from (m), showing that it is more like dura than arachnoid. (o) Once the array from (n) was removed, a thick bed of encapsulation tissue was seen below and was clearly continuous with the dura.

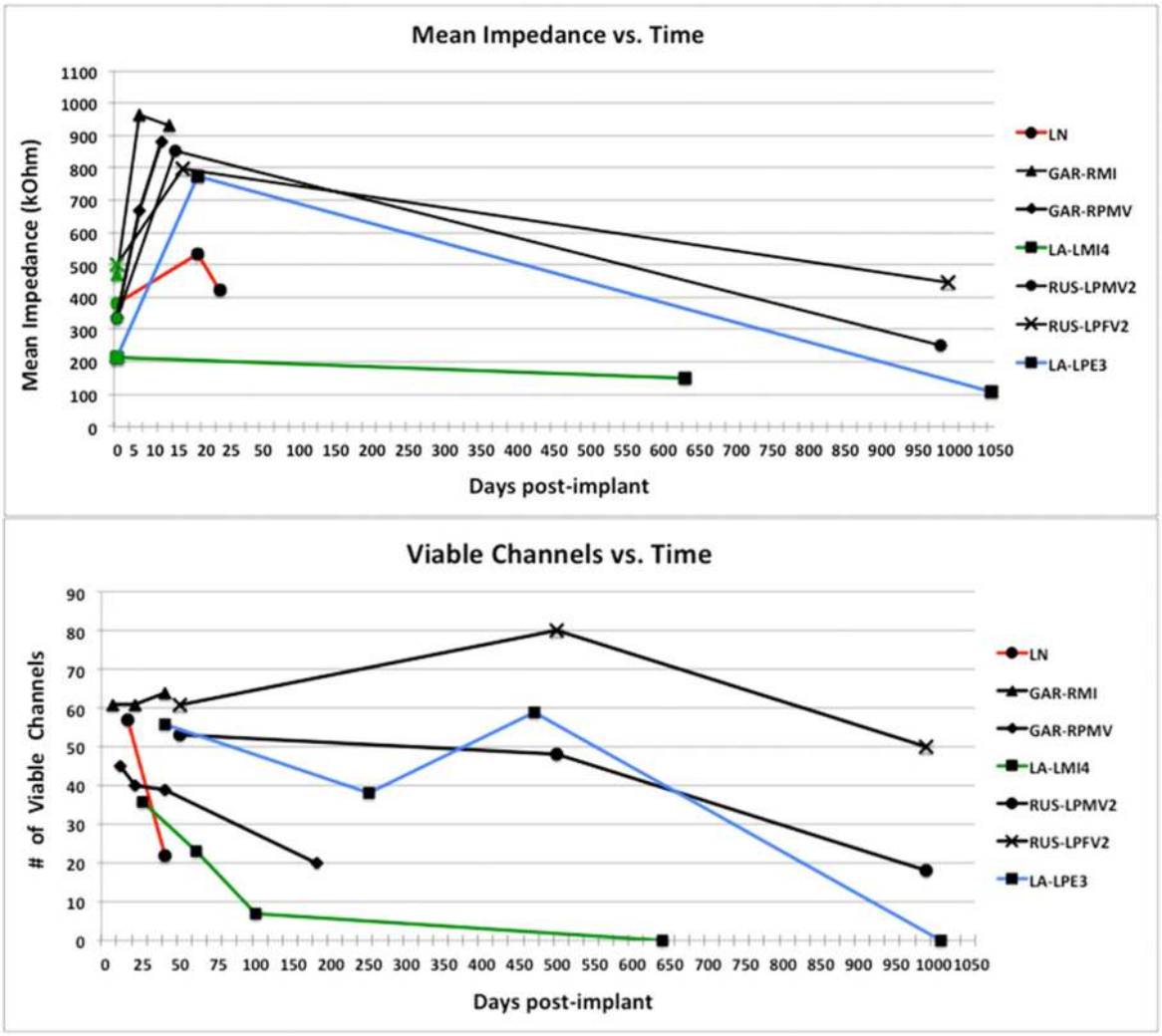

Figure 3.

Neural recordings. *Top*: mean impedance (kOhm) over time (days post-implant). Initial (pre-implant) values are plotted at day 0 with green markers. Scale for the first 50 days is expanded to show the early rise in impedance. *Bottom*: the number of viable channels on each array over time (days post-implant). Failure modes are indicated by line color. Red = acute biological, blue = chronic unknown, green = chronic biological, black = acute mechanical.

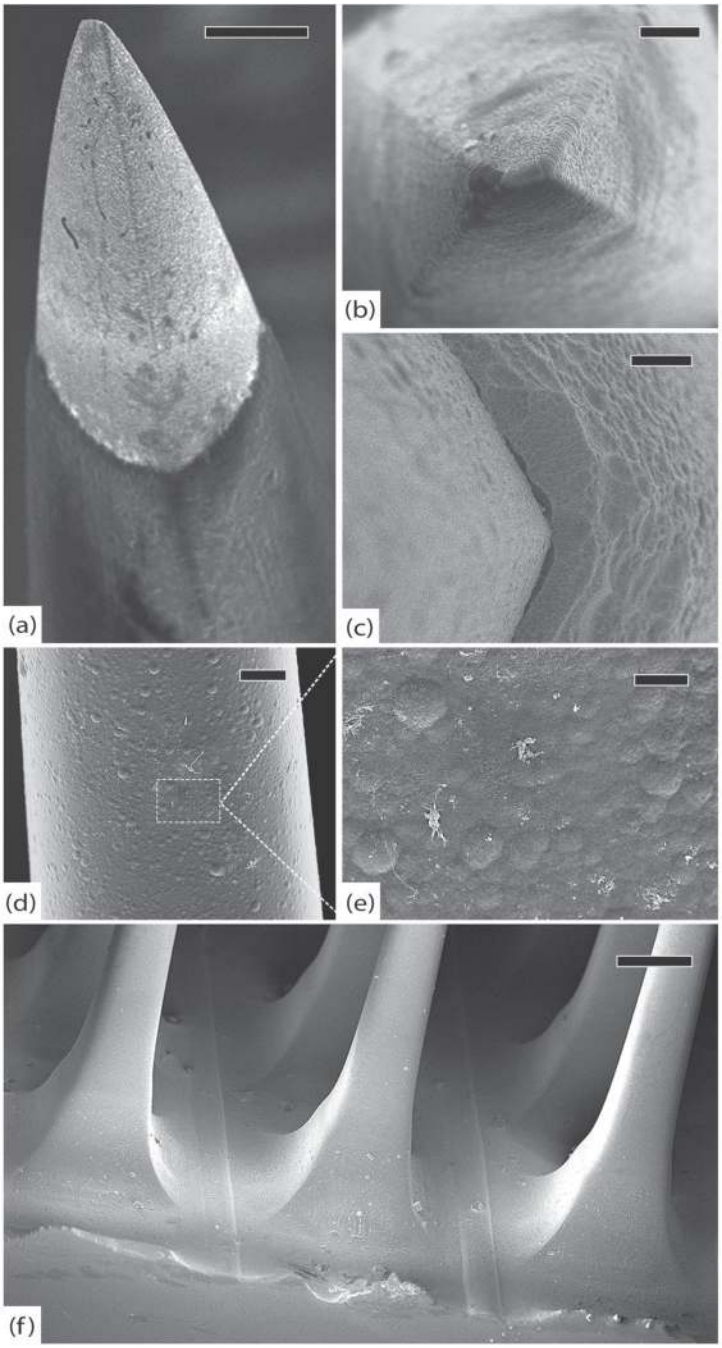

Figure 4.

Control arrays. (a) Control array 1 (CA1), representative tip showing platinum/parylene border, scale 10 μm. (b) CA1, another normal tip showing pyramidal geometry of electrodes, scale 2 μm. (c) Control array 2 (CA2), normal platinum/parylene interface without delamination, scale 1 μm. (d) Control array 3 (CA3), normal appearance of parylene along an electrode shaft, scale 10 μm. (e) Close-up of parylene surface from (d) showing characteristic surface irregularities, scale 2 μm. (f) CA3, edge of the array, note that there is

no silicone elastomer on this array and there are no cracks in the parylene, scale 100 μm. All images in this figure were taken at 5 kV.

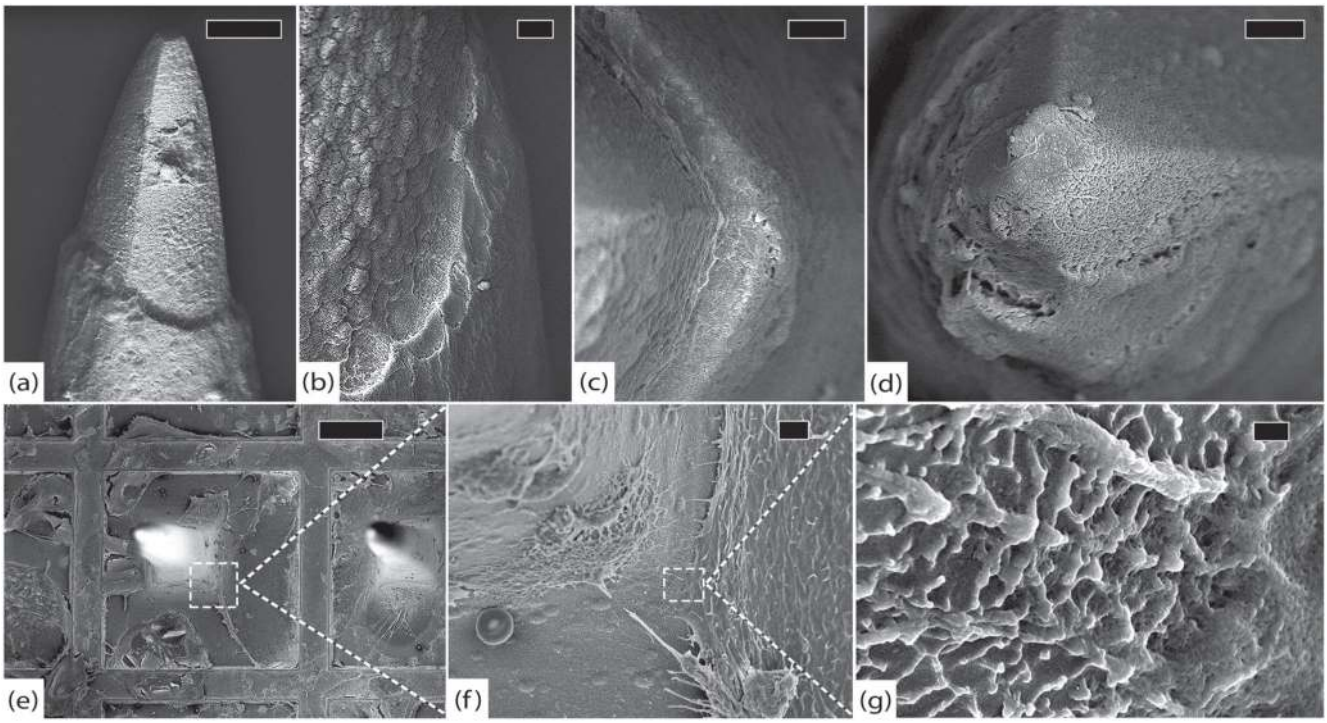

Figure 5.

LN-LSMA, 37 days (a) electrode tip with thin film of encapsulation tissue, scale 10 μm. (b) Platinum/parylene interface without delamination, scale 1 μm. (c) The platinum/parylene interface of another electrode at a different angle showing no significant delamination and a thin layer of fibrosis, scale 2 μm. (d) Intact platinum electrode tip partially covered with encapsulation tissue approx. 250 nm thick, scale 2 μm. (e) Active macrophages and fibroblasts along the base of the array, scale 100 μm. (f) Close-up at base of electrode from (e) showing active tissue growth (and an erythrocyte), scale 5 μm. (g) Higher magnification of encapsulation tissue from (f) showing individual collagen fibers, scale 200 nm. All images in this figure were taken at 5 kV.

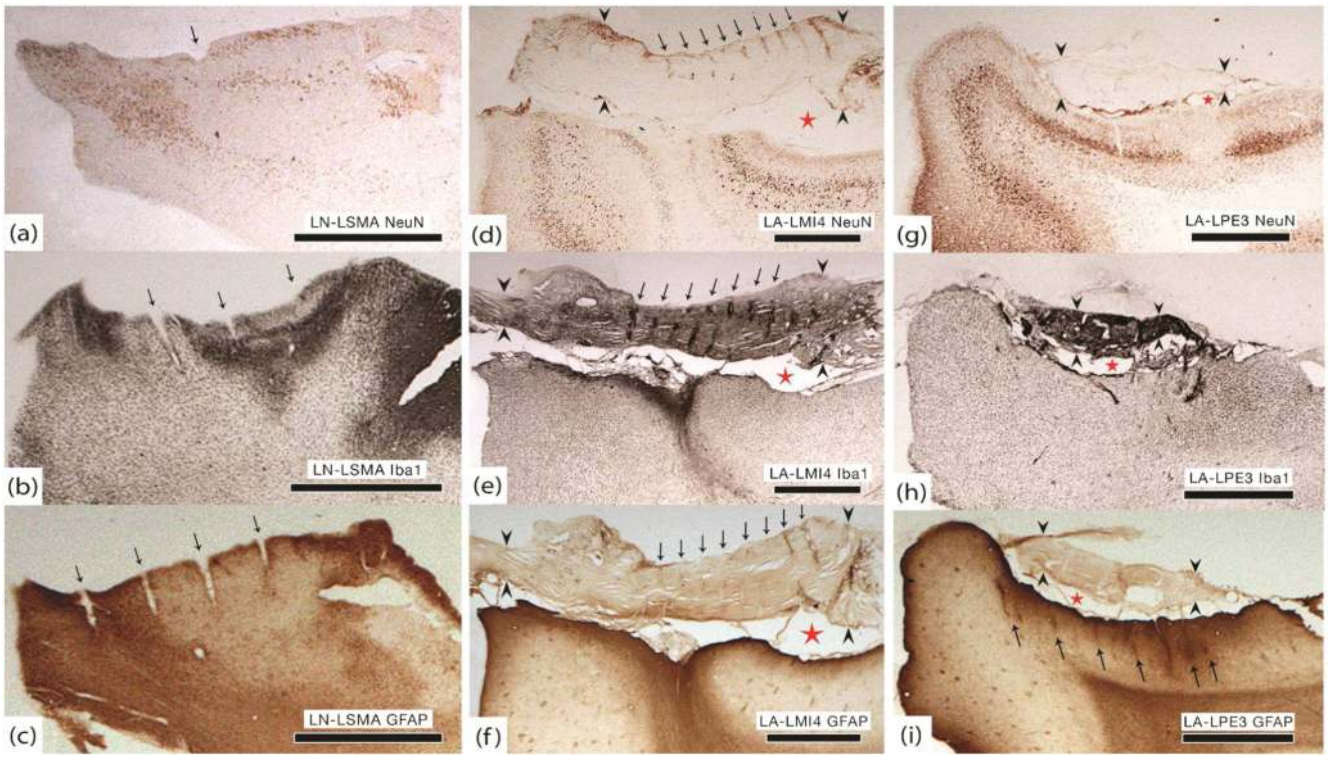

Figure 6.

Histology. All sections were prepared in the coronal plane. Black arrows point to electrode tracts, red stars indicate the subarachnoid space, and black arrowheads bracket the dura. (a) LN-LSMA. Decreased NeuN staining within implant site. This may be an artifact because the entire specimen was poorly stained, including areas far from the implant site. (b) LN-LSMA. Clear region of increased Iba1 activity within implant site. (c) LN-LSMA. Increased GFAP staining at the edges of the implant site. The dura and arachnoid were not preserved and therefore they are not visible in panels (a)–(c). (d) LA-LMI4. Significant decrease in NeuN staining and loss of normal cortical architecture. (e) LA-LMI4. Dense Iba1 activity at the center of the implant site and within dural encapsulation tissue, especially around electrode tracts (black arrows). (f) LA-LMI4. Increased GFAP staining and a dense glial scar at the center of the implant site. No evidence of electrode tracts in the cortex although they are seen in the dura (black arrows). (g) LA-LPE3. Only a small region of decreased NeuN staining within the implant site. (h) LA-LPE3. Dense Iba1 activity within arachnoid and dura (black arrowheads). Increased activity within the implant site at the same location where neuronal density was diminished. (i) LA-LPE3. A thick layer of gliosis is present throughout the implant site and partial electrode tracts are identified (black arrows). The densest region of GFAP staining correlates to high Iba1 and low NeuN staining. All scale bars in this figure are 2 mm.

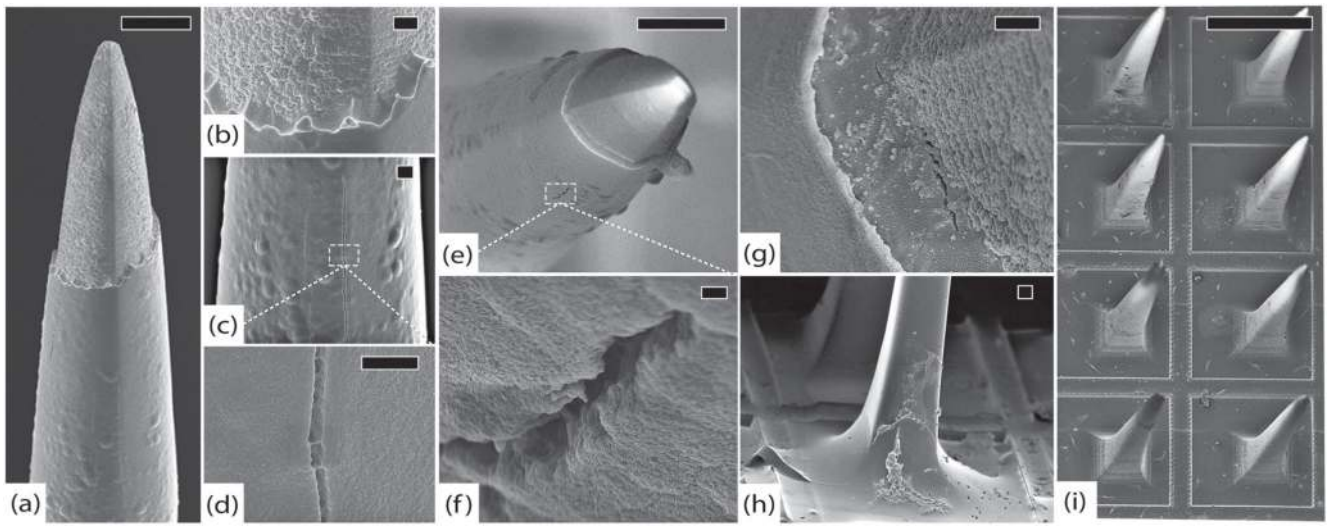

Figure 7.

SCT-RVI, 99 days. (a) Representative electrode tip, scale 20 μm. (b) Detail of electrode from (a) showing intact platinum and no delamination at the parylene interface, scale 2 μm. (c) Closer view of electrode from (a) showing longitudinal cracks in the parylene, scale 2 μm. (d) Detail of parylene crack, scale 2 μm. (e) Another typical electrode with intact platinum and minimal encapsulation, scale 20 μm. (f) Detail of cracked parylene, scale 300 nm. (g) Closer view of parylene interface showing early delamination and a thin veil of encapsulation tissue, scale 1 μm. (h) Base of an electrode with fibroblasts along the shaft. There is a distinct layer of encapsulation tissue creeping up the electrode, scale 20 μm. (i) Globular macrophages and spindle-shaped fibroblasts are visible on the base of the array, scale 300 μm. All images in this figure were taken at 5 kV.

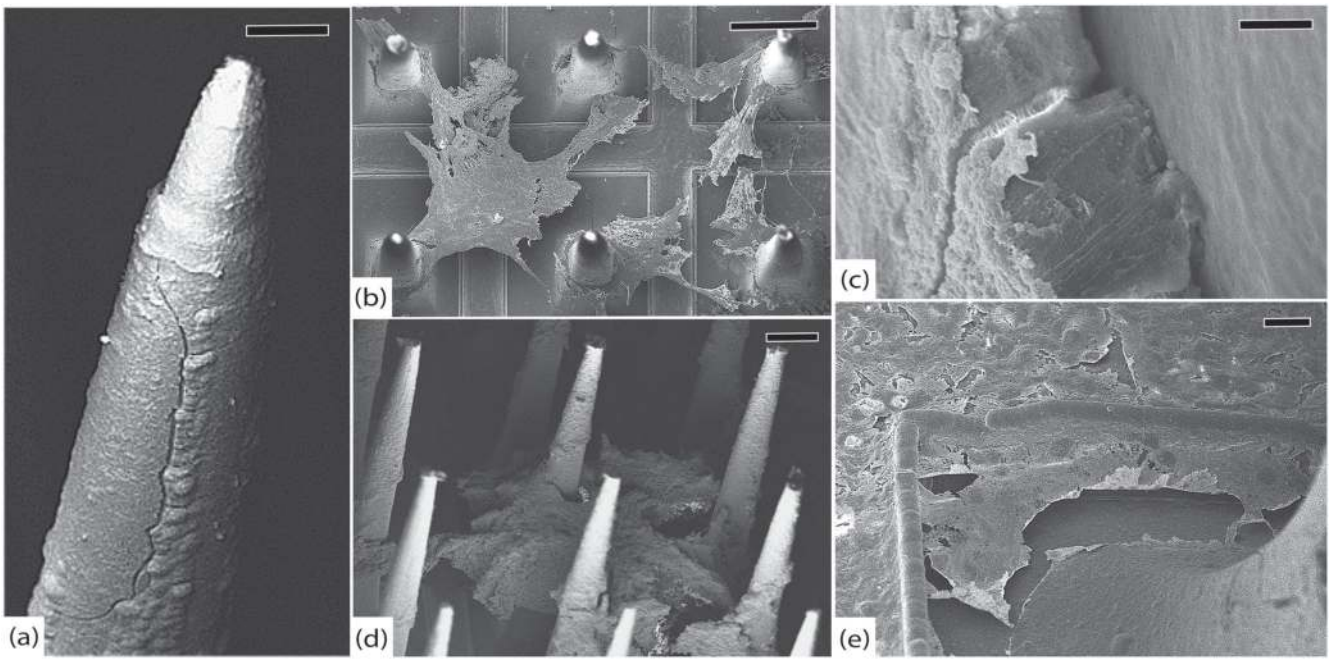

Figure 8.

GAR-RMI, 554 days. (a) Side view of an electrode with a large longitudinal crack in the parylene adjacent to surface irregularities, scale 20 μm. (b) Top view of array showing sheets of fibrosis suspended between electrodes, scale 200 μm. (c) Cracked parylene along an electrode shaft with underlying silicon exposed and tissue invasion, scale 1 μm. (d) Side view of the array showing thick fibrous tissue suspended between electrodes. Note that the tissue is adherent halfway up the shaft, indicating that the electrode tips were not fully seated in the cortex, scale 100 μm. (e) A thin film of collagen is present along the base of the array. A crack in the parylene is also visible underneath this encapsulation tissue, scale 10 μm. All images in this figure were taken at 5 kV.

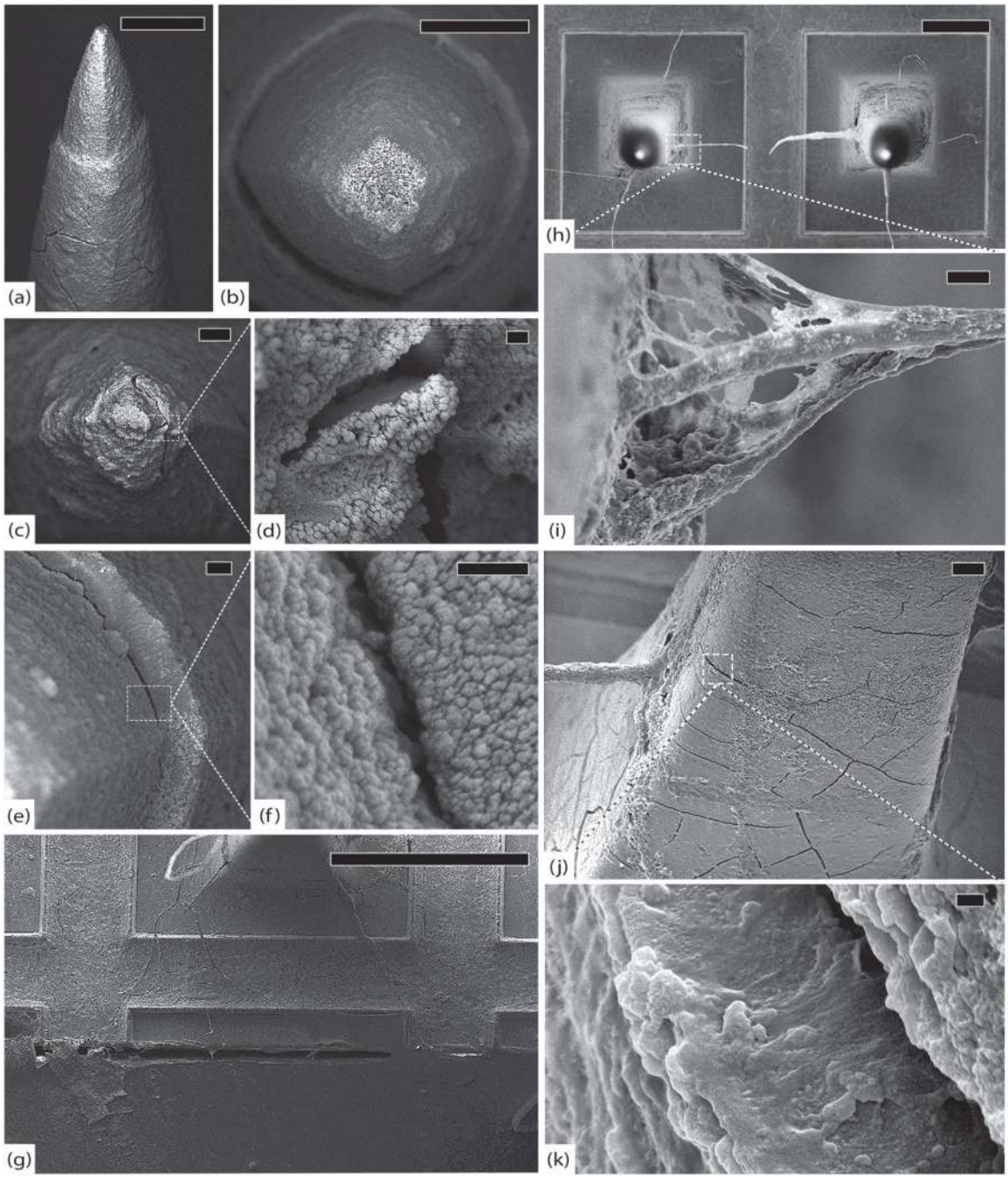

Figure 9.

GAR-RPMv, 554 days. (a) Side view of a typical electrode with intact platinum, cracked parylene and substantial fibrosis, scale 20 μm. (b) Top view of another typical electrode with intact platinum and thick, uniform fibrous encapsulation, scale 10 μm. (c) An electrode tip with thick encapsulation tissue, scale 3 μm. (d) Detail of cracked platinum tip, scale 200 nm. (e) Delaminating parylene interface, scale 1 μm. (f) Detail of parylene delamination, scale 200 nm. (g) Edge of the array showing silicone elastomer peeling away from parylene, scale 200 μm. (h) Top view of array showing large collagen fibers suspended between electrodes,

scale 100 μm. (i) Detail of elastic collagen fiber attached to the shaft of an electrode, scale 3 μm. (j) An electrode shaft showing adherent elastic collagen fiber and abundant cracks in parylene, scale 10 μm. (k) Detail of a full-thickness transverse crack in parylene with tissue invasion, scale 200 nm. All images in this figure were taken at 5 kV.

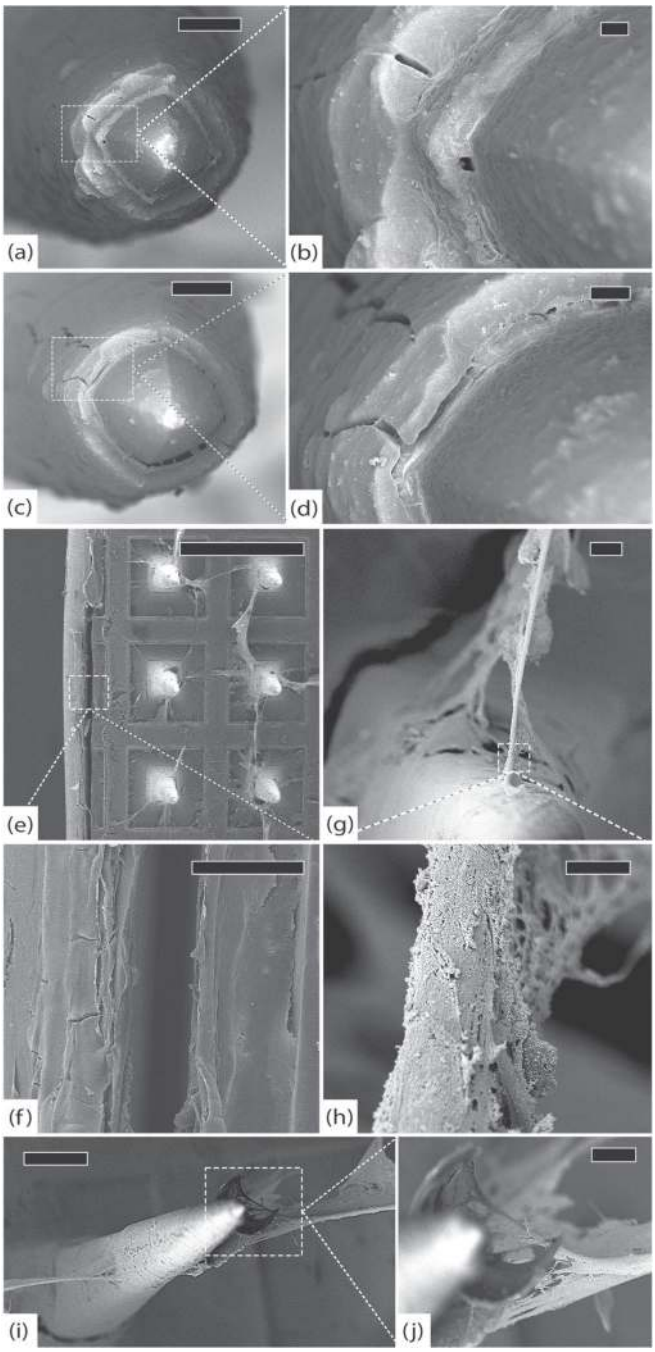

Figure 10.

LA-LMI4, 639 days. (a) Typical electrode tip with intact platinum and thick encapsulation, scale 10 μm, 3 kV. (b) Detail of parylene interface where a longitudinal crack is seen but delamination cannot be assessed because the interface is obscured by fibrosis, scale 1 μm, 3 kV. (c) Another electrode with intact platinum and clear delamination, scale 10 μm, 3 kV. (d) Detail showing cracked parylene and delamination with tissue invasion, scale 2 μm, 3 kV. (e) Silicone delaminating from parylene at the edge of the array, scale 500 μm, 8 kV. (f) Detail of silicone delamination and thin film of fibrosis on the base, scale 50 μm, 8 kV. (g) Elastic

collagen fibers attached to the shaft of an electrode, scale 10 μm, 3 kV. (h) Detail of collagen fiber showing individual collagen fibrils, scale 2 μm, 3 kV. (i) Inter-electrode fibrosis peeling parylene off the electrode shaft, scale 100 μm, 3 kV. (j) Detail of collagen fibers enveloping a segment of parylene, pulling it away from the electrode, scale 20 μm, 3 kV.

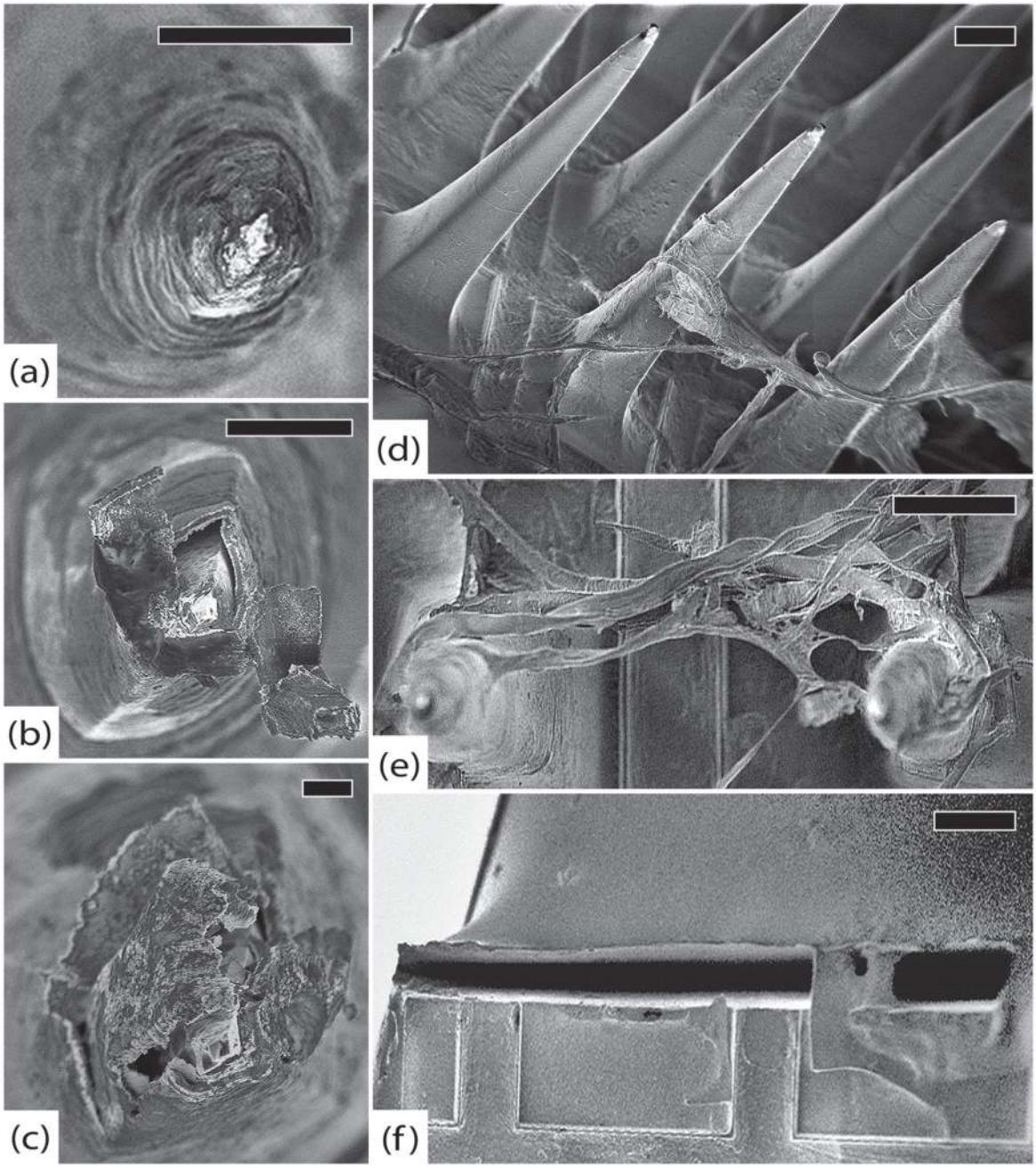

Figure 11.

RUS-LPMv2, 994 days. (a) An electrode tip completely covered in a thick layer of fibrosis, scale 20 μm. (b) Another electrode showing platinum peeling off of underlying silicon. Encapsulation tissue is intermingled with platinum fragments and there are linear defects in the platinum. These findings may be due to mechanical shearing as the array was removed from the brain, scale 10 μm. (c) An electrode with thick encapsulation tissue adherent to platinum that has separated from the silicon, scale 2 μm. (d) Side view of the array showing thick encapsulation tissue, inter-electrode fibrosis, elastic collagen fibers, and cracked parylene, scale 100 μm. (e) Thick tangle of elastic collagen fibers between electrodes in the

center of the array, scale 100 μm. (f) Separation between the silicone elastomer of the wire bundle and the parylene at the edge of the array, scale 100 μm. All images in this figure were taken at 1 kV.

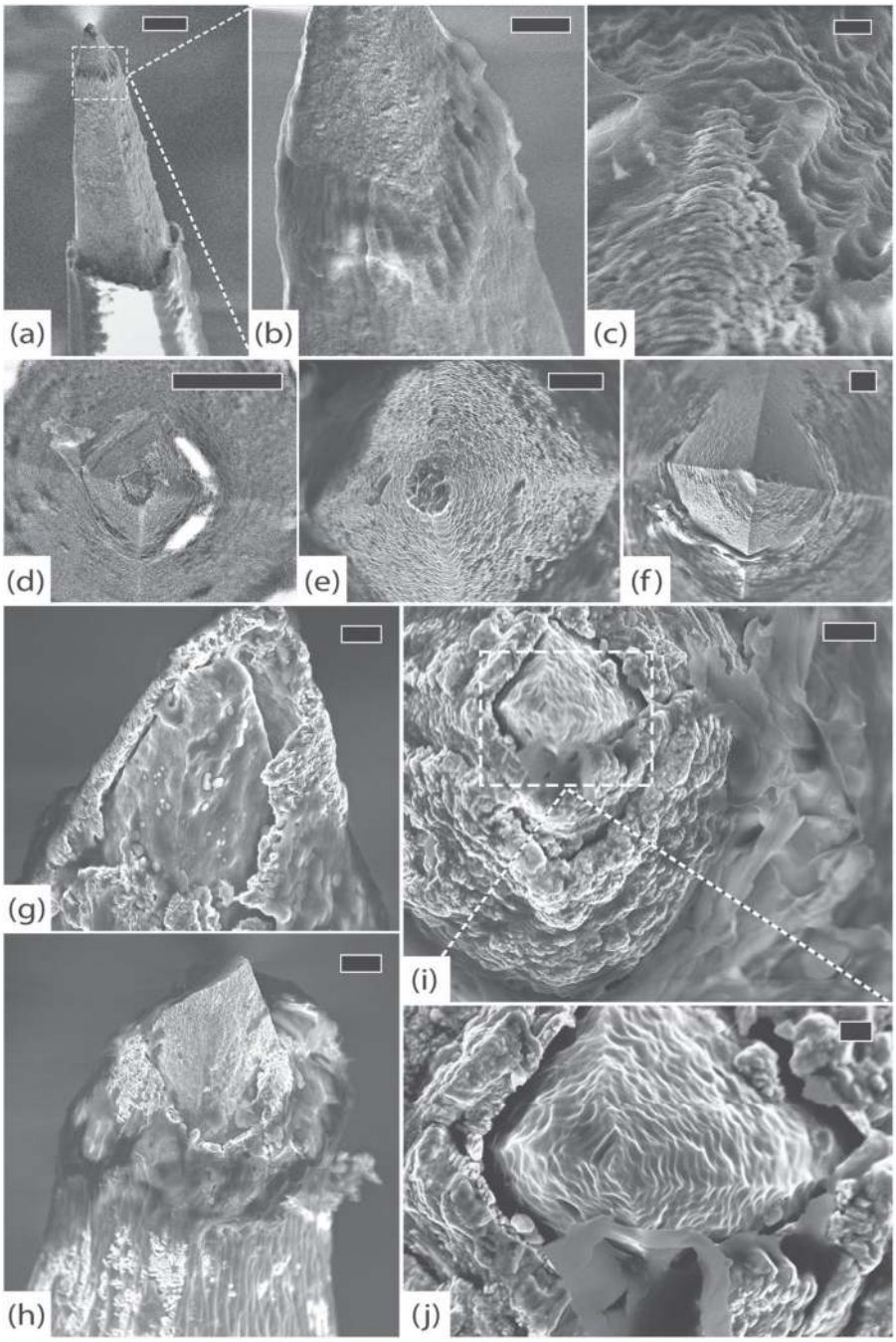

Figure 12.

RUS-LPFv2, 994 days. (a) An electrode with significant delamination at parylene interface and thick fibrosis at the tip, scale 10 μm, 10 kV. (b) Detail of encapsulation showing individual collagen fibers, scale 3 μm, 10 kV. (c) Top view of another electrode showing collagenous tissue growth (top) along platinum tip (bottom), scale 300 nm, 5 kV. (d) Top view of an electrode with damaged platinum tip and exposed silicon, scale 10 μm, 5 kV. (e) Top view of another electrode with an essentially intact platinum tip, scale 2 μm, 5 kV. (f) Top view of a severely degraded electrode tip. The platinum is almost completely

disintegrated and the silicon beneath it shows signs of pitting corrosion. Note that there is no evidence of mechanical damage, indicating a chronic process, scale 2 μm, 5 kV. (g) Side view of yet another electrode with severe platinum corrosion, exposure of underlying silicon, and tissue invasion, scale 1 μm, 5 kV. (h) An electrode with thick fibrous encapsulation that appears to be peeling the platinum away from the exposed silicon, scale 2 μm, 5 kV. (i) Top view of a different electrode showing a swollen, possibly oxidized, platinum layer that has separated from the underlying silicon, scale 1 μm, 5 kV. (j) Detail of tissue growth between the exposed silicon and platinum, scale 200 nm, 5 kV.

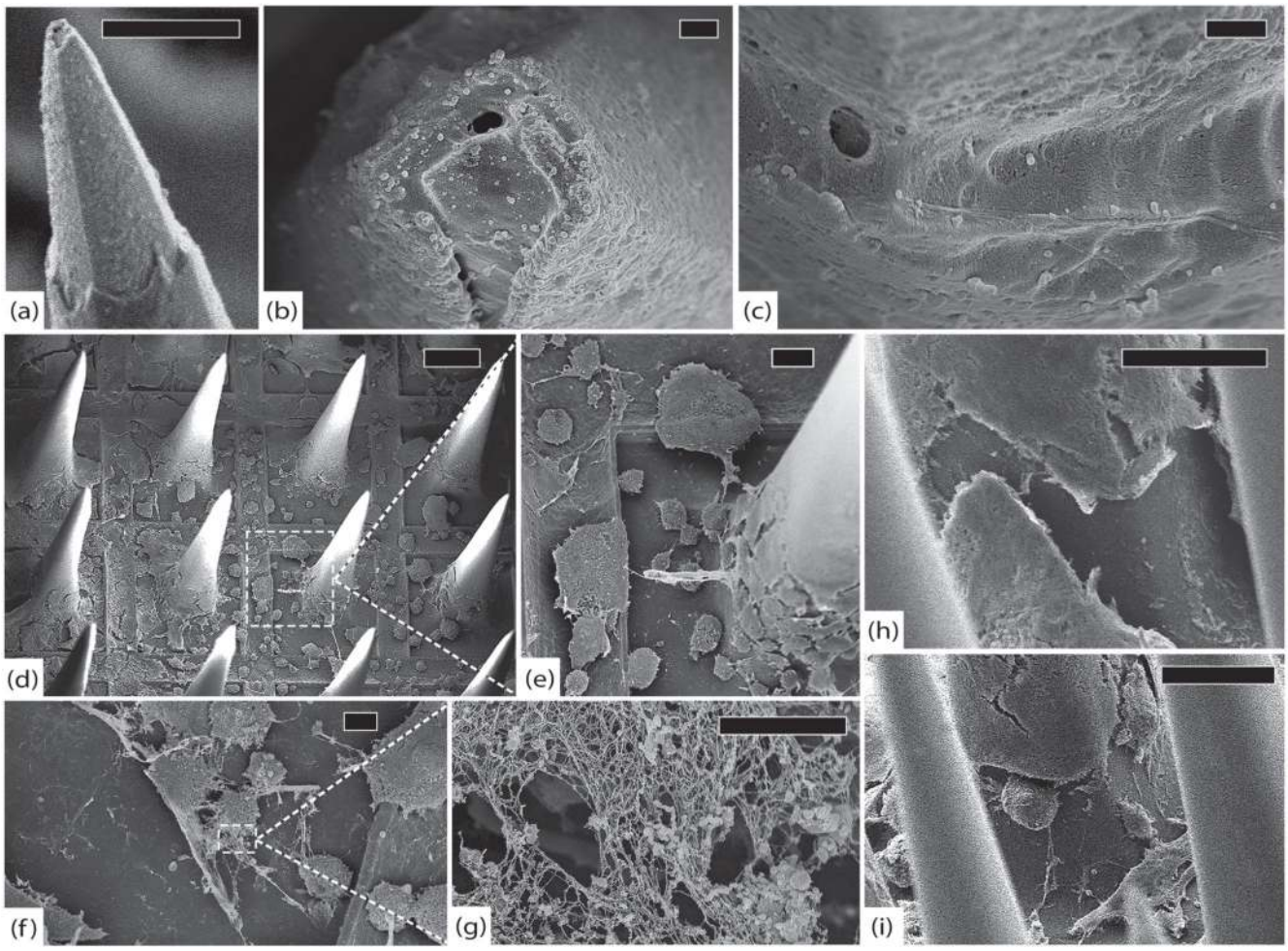

Figure 13.

LA-LPE3, 1051 days. (a) A typical electrode tip with thick encapsulation and minimal platinum tip degradation, scale 30 μm, 8 kV. (b) Top view of another electrode tip showing platinum erosion, silicon exposure, and tissue invasion, scale 1 μm, 5 kV. (c) Top view of parylene interface where delamination is difficult to assess because of thick fibrosis, scale 1 μm, 5 kV. (d) Top view of array showing abundant cellular material and thick fibrotic encapsulation, scale 200 μm, 5 kV. (e) Detail showing numerous cells at the base of an electrode with remnants of larger inter-electrode collagen fibers, scale 30 μm, 5 kV. (f) Close-up of fibroblasts on the base, scale 10 μm, 5 kV. (g) Detail showing individual collagen fibrils that compose encapsulation tissue, scale 2 μm, 5 kV. (h) Side view of an electrode shaft with thick fibrotic encapsulation tissue, scale 70 μm, 8 kV. (i) Side view of another electrode with fibroblasts actively depositing collagen, scale 100 μm, 8 kV.

J Neural Eng. Author manuscript; available in PMC 2016 May 03.

Table 1

Summary of implant durations, neural recordings, clinical events, histology, and failure modes.

Array name	Time *in vivo*	Neural recordings: mean value (*day post-implant*)	Clinical events	Histology	Failure mode
Control 1	N/A	N/A	N/A	N/A	N/A
Control 2	N/A	N/A	N/A	N/A	N/A
Control 3	N/A	N/A	N/A	N/A	N/A
LN-LSMA	37 days	IMP (kOhm)—380 (0), 533 (15), 424 (20)			
		AMP (μV)—80 (15), 64 (36)	Euthanized at 37 days, array removed from brain after perfusion	Thin arachnoid encapsulation, increased Iba1 throughout and GFAP at the edges. NeuN stained poorly	Acute biological—euthanization
		Namp (μV)—45 (15), 45 (36)			
		SNR—1.8 (15), 1.4 (36)			
		VC (#)—57 (15), 22 (36)			
SCT-RV1	99 days	N/A	Failed within a week for unknown reasons. Explanted at 99 days	Fibrous capsule adherent to dura with thin electrode tracts diving into cortex	Acute unknown—likely mechanical
		Failed within first week, high amplitude noise. No IMPs available.			
GAR-RMI	554 days	IMP (kOhm)—470 (0), 963 (4), 931 (8)			
		AMP (μV)—79 (7), 90 (18), 83 (39)	Internalized (wire bundle cut at skull) at 119 days, Explanted at 554 days	Dense fibrous capsule adherent to dura with soft inflamed tissue below array	Acute mechanical—surgical internalization
		Namp (μV)—61 (7), 64 (18), 57 (39)			
		SNR—1.3 (7), 1.4 (18), 1.5 (39)			
		VC (#)—61 (7), 61 (18), 64 (39)			
GAR-RPMV	554 days	IMP (kOhm)—340 (0), 670 (4), 898 (8)			
		AMP (μV)—72 (7), 80 (18), 66 (39), 55 (175)	Internalized (wire bundle cut at skull) at 176 days, Explanted at 554 days	Dense fibrous capsule adherent to dura with thick electrode tracts diving into cortex	Acute mechanical—surgical internalization
		Namp (μV)—47 (7), 49 (18), 38 (39), N/A (175)			
		SNR—1.5 (7), 1.6 (18), 1.7 (39), N/A (175)			
		VC (#)—45 (7), 40 (18), 39 (39), 20 (175)			
LA-LMI4	639	IMP (kOhm)—214 (0), 149 (639)			

Array name	Time *in vivo*	Neural recordings: mean value (*day post-implant*)	Clinical events	Histology	Failure mode
	days	AMP (μV)—94 (21), 71 (59), 60 (99)	Failed around 99 days. Array explanted at 639 days (prior to perfusion)	Completely intradural electrodes, high GFAP and Iba1 reactivity, NeuN showed loss of layered cortical structure	Chronic biological—meningeal encapsulation and extrusion, possibly neuronal cell death
		Namp (μV)—45 (21), 39 (59), 32 (99)			
		SNR—2.1 (21), 1.8 (59), 1.9 (99)			
		VC (#)—37 (21), 23 (59), 7 (99), 0 (639)			
RUS-LPMV2	994 days	IMP (kOhm)—335 (0), 855 (9), 251 (976)			
		AMP (μV)—101 (50), 86 (499), 70 (990)	Functional array explanted at 994 days in order to conduct alternate experiment	Thick dural encapsulation surrounding array and partially lifting it from the cortex	Acute mechanical—surgical removal
		Namp (μV)—51 (50), 48 (499), 40 (990)			
		SNR—2 (50), 1.7 (499), 1.8 (990)			
		VC (#)—53 (50), 48 (499), 18 (990)			
RUS-LPFV2	994 days	IMP (kOhm)—500 (0), 795 (8), 466 (990)			
		AMP (μV)—93 (51), 73 (499), 71 (990)	Functional array explanted at 994 days in order to conduct alternate experiment	Thick dural encapsulation surrounding array	Acute mechanical—surgical removal
		Namp (μV)—58 (51), 47 (499), 45 (990)			
		SNR—1.6 (51), 1.5 (499), 1.7 (990)			
		VC (#)—61 (51), 80 (499), 50 (990)			
		IMP (kOhm)—214 (0), 774 (14), 106 (1051)			
LA-LPE3	1051 days	AMP (μV)—81 (41), 55 (252), 53 (471)	Failed by 1008 days, explanted at 1051 days (prior to perfusion)	High GFAP, focal loss of NeuN, thick dural capsule with intense Iba1, array partially extruded, minimal electrode tracts in cortex	Chronic unknown—likely a combination of fibrous encapsulation, electrode corrosion, and parylene failure
		Namp (μV)—50 (41), 41 (252), 42 (471)			
		SNR—1.6 (41), 1.3 (252), 1.3 (471)			
		VC (#)—56 (41), 38 (252), 59 (471), 0 (1008)			

Note: Abbreviations: impedance (IMP), amplitude (AMP), noise amplitude (Namp), signal-to-noise ratio (SNR), number of viable channels (VC).

Table 2

Summary of array time *in vivo*, processing techniques, and SEM imaging results.

Array name	Time *in vivo*	SEM prep	SEM findings
Control 1	N/A	No fixation, critical point dryer, Au/Pd coating	Tips: No platinum degradation; minimal parylene delamination.
			Shafts: No cracks in parylene, rare parylene irregularities.
			Base: No cracks in parylene, rare parylene irregularities.
			Edges: No silicone deposited, no cracks in parylene or silicon.
Control 2	N/A	NaCl × 1 wk, critical point dryer, Au/Pd coating	Tips: No platinum degradation; minimal parylene delamination.
			Shafts: No cracks in parylene, rare parylene irregularities.
			Base: No cracks in parylene, rare parylene irregularities.
			Edges: No silicone deposited, no cracks in parylene or silicon.
Control 3	N/A	NaCacodylate × 1 wk, critical point dryer, Au/Pd coating	Tips: No platinum degradation; minimal parylene delamination.
			Shafts: No cracks in parylene, rare parylene irregularities.
			Base: No cracks in parylene, rare parylene irregularities.
			Edges: No silicone deposited, no cracks in parylene or silicon.
LN- LSMA	37 days	NaCacodylate fix, ethanol, critical point dryer, Au/Pd coating	Tips: No platinum degradation; thin tissue encapsulation (~250 nm); no parylene delamination.
			Shafts: Thin uniform tissue encapsulation with many fibroblasts; few cracks in parylene.
			Base: Many active macrophages and fibroblasts; occasional shallow cracks in parylene.
			Edges: No silicone delamination, no cracks; no tissue adhesions or cells on silicone.
SCT-RV1	99 days	NaCacodylate fix, ethanol, critical point dryer, Au/Pd coating	Tips: No platinum degradation; thin partial tissue encapsulation (~250 nm); no parylene delamination.
			Shafts: Irregular, thin tissue encapsulation (~250 nm) with few cells; several longitudinal parylene cracks; no collagen fibers.
			Base: Many cells at base, few cracks in parylene.
			Edges: No silicone delamination, rare cracks, few tissue adhesions on silicone.
GAR-RMI	554 days	NaCacodylate fix, ethanol, critical point dryer, Au/Pd coating	Tips: No platinum degradation; complete tissue encapsulation (~250–500 nm); rare parylene delamination.
			Shafts: Irregular, thick tissue adhesions (~1–5 μm) with many fibroblasts; many cracks in parylene, often with tissue invasion; many collagen fibers, often connecting adjacent electrodes (central>peripheral).
			Base: Few cells, thin fibrous layer (~250 nm); few cracks in parylene, most shallow.
			Edges: Rare silicone delamination, no cracks; few tissue adhesions found on silicone.
GAR-RPMV	554 days	NaCacodylate fix, ethanol, critical point dryer, Au/Pd coating	Tips: Few cracked platinum tips; complete tissue encapsulation (~250–500 nm); some parylene delamination.

Array name	Time *in vivo*	SEM prep	SEM findings
			Shafts: Irregular, thick tissue adhesions (~1–5 μm) with many fibroblasts; many transverse cracks in parylene, often with tissue invasion; many collagen fibers, often connecting adjacent electrodes.
			Base: Few cells; thin fibrous layer (~250 nm) many shallow cracks in parylene, some deep.
			Edges: Minor silicone delamination, no cracks; few tissue adhesions on silicone.
LA-LMI4	639 days	NaCacodylate fix, ethanol, critical point dryer, Au/Pd coating	Tips: No platinum degradation; complete tissue encapsulation (250–500 nm); abundant parylene delamination.
			Shafts: Irregular, thick tissue encapsulation (>500 nm) with many fibroblasts; many cracks in parylene with tissue invasion; many collagen fibers between adjacent electrodes (central>peripheral); parylene often peeled off by tissue.
			Base: Few cells, thick fibrous layer (~500 nm–1 μm); many deep cracks in parylene.
			Edges: Abundant silicone delamination and cracks; numerous tissue adhesions on silicone.
RUS-LPMV2	994 days	NaCacodylate fix, ethanol, critical point dryer, no sputter-coating	Tips: Widespread platinum degradation (>50% of electrodes) with many cracks, often with separation of platinum from silicon and erosion of underlying silicon; thick complete tissue encapsulation (~500 nm) with growth between platinum and silicon; minimal parylene delamination.
			Shafts: Regular, thick tissue encapsulation (>500 nm) with few cells; few parylene cracks; many collagen fibers throughout array, often connecting adjacent electrodes.
			Base: Many cells, thick fibrous layer (500 nm–1 μm); few cracks in parylene.
			Edges: No cracks, 1 mm of silicone delamination at junction of wire bundle; many tissue adhesions on silicone.
RUS-LPFV2	994 days	NaCacodylate fix, ethanol, critical point dryer, no sputter-coating	Tips: Extensive platinum degradation (>66% of electrodes) with many cracks and erosion of underlying silicon; thick complete tissue encapsulation (>500 nm) with growth between platinum and silicon; some parylene delamination.
			Shafts: Regular, thick tissue encapsulation (>500 nm) with few cells; rare parylene cracks; rare collagen fibers.
			Base: Many cells, thick fibrous layer (500 nm–1 μm); few cracks in parylene.
			Edges: Few segments of silicone delamination, few cracks; many tissue adhesions on silicone.
LA-LPE3	1051 days	NaCacodylate fix, ethanol, critical point dryer, Au/Pd coating	Tips: Extensive platinum degradation (>95% of electrodes) with many cracks and erosion of underlying silicon; thick complete tissue encapsulation (>500 nm) with growth between platinum and silicon; some parylene delamination.
			Shafts: Regular, thick tissue encapsulation (500 nm–1 μm) with few cells; few cracks in; no collagen fibers.
			Base: Many cells that merge into thick fibrous layer (1–5 μm) as they ascend shafts; few cracks in parylene.
			Edges: Minimal silicone delamination, few cracks; many tissue adhesions on silicone.